ARTICLE

Discovery of nitrate–CPK–NLP signalling in central nutrient–growth networks

Kun-hsiang Liu[1,2]*, Yajie Niu[1]*, Mineko Konishi[3], Yue Wu[1], Hao Du[1], Hoo Sun Chung[1], Lei Li[1], Marie Boudsocq[1,4], Matthew McCormack[1], Shugo Maekawa[3], Tetsuya Ishida[3], Chao Zhang[5], Kevan Shokat[5], Shuichi Yanagisawa[3] & Jen Sheen[1]

Nutrient signalling integrates and coordinates gene expression, metabolism and growth. However, its primary molecular mechanisms remain incompletely understood in plants and animals. Here we report unique Ca^{2+} signalling triggered by nitrate with live imaging of an ultrasensitive biosensor in *Arabidopsis* leaves and roots. A nitrate–sensitized and targeted functional genomic screen identifies subgroup III Ca^{2+}-sensor protein kinases (CPKs) as master regulators that orchestrate primary nitrate responses. A chemical switch with the engineered mutant CPK10(M141G) circumvents embryo lethality and enables conditional analyses of *cpk10 cpk30 cpk32* triple mutants to define comprehensive nitrate–associated regulatory and developmental programs. Nitrate–coupled CPK signalling phosphorylates conserved NIN–LIKE PROTEIN (NLP) transcription factors to specify the reprogramming of gene sets for downstream transcription factors, transporters, nitrogen assimilation, carbon/nitrogen metabolism, redox, signalling, hormones and proliferation. Conditional *cpk10 cpk30 cpk32* and *nlp7* mutants similarly impair nitrate–stimulated system–wide shoot growth and root establishment. The nutrient–coupled Ca^{2+} signalling network integrates transcriptome and cellular metabolism with shoot–root coordination and developmental plasticity in shaping organ biomass and architecture.

Nitrate is the primary nitrogen source for most plants and the limiting factor for growth in aerobic soil[1–3]. Nitrate rapidly stimulates integrated nutrient transport and assimilation, as well as carbon/nitrogen metabolic and regulatory pathways that enable plant growth plasticity to respond and adapt to fluctuating environments. Genetic and genomic evidence suggest that nitrate drives rapid transcriptional regulation and that nitrate signalling is uncoupled from nitrate metabolism[1,3–17]. Regulatory components in nitrate sensing and signalling, such as the NRT1.1 (also known as NPF6.3, CHL1 and NRG1) transceptor and associated calcineurin-B-like-interacting protein kinases (CIPKs) and protein phosphatase 2C (PP2C, also known as ABI2), as well as nitrate-responsive *cis*-elements (NREs) and transcription factors, have been identified by molecular, genetic, genomic and systems analyses[2–21]. Notably, *Arabidopsis* NLP6 and NLP7 have been implicated as key transcription factors of primary nitrate responses[3,9,12,13]. Despite these advances, the molecular mechanism underlying primary nitrate signalling downstream of multiple sensors to integrated transcription, transport, metabolism and systemic growth programs (Fig. 1a) remains unclear[1–3,6,7,11,18,21].

Ca^{2+} is an evolutionarily conserved and versatile signalling modulator in diverse regulatory pathways, such as stress, immune and neuron signalling[22–27]. Although a role for Ca^{2+} signalling in nitrate-responsive gene regulation has been implicated in maize leaves and *Arabidopsis* roots[28,29], many outstanding questions remain in both plants and animals, such as whether distinct Ca^{2+} signatures are involved in primary nutrient signalling with cell specificity, the specific patterns of Ca^{2+} dynamics, the identity of intracellular Ca^{2+} sensors, how Ca^{2+} sensors relay signalling specificity, and the downstream targets of Ca^{2+} signalling in the nutrient–growth regulatory networks.
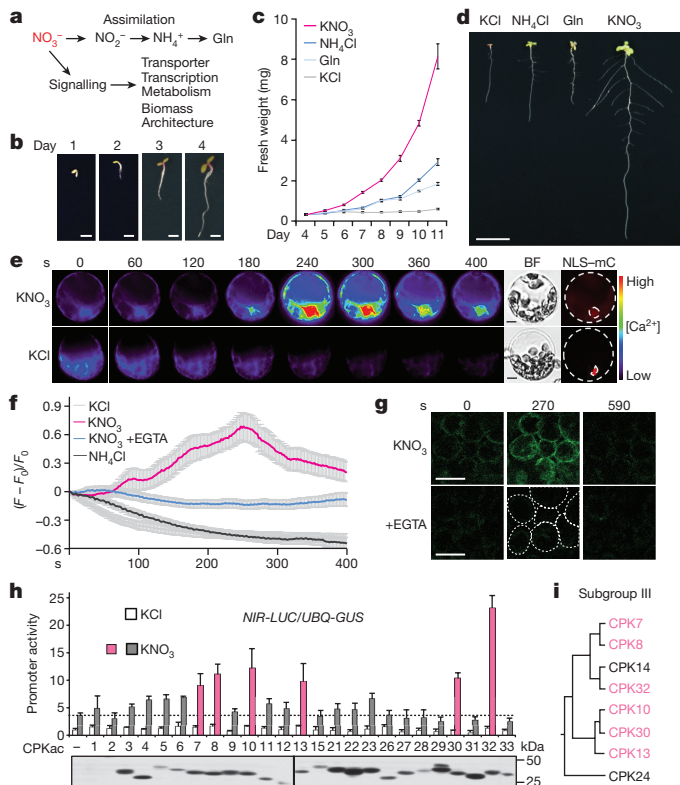
Nitrate triggers unique Ca^{2+}–CPK signalling

To determine the primary mechanism in nitrate signalling, we developed integrated seedling and cell-based assays in *Arabidopsis*. Without exogenous nitrogen, seed reserves supported rapid initial seedling growth after germination (Fig. 1b). However, the increase in biomass ceased after four days even with illumination and sucrose supplies (Fig. 1c, d). Although ammonium (NH_4^+) or glutamine (Gln) was transported, sensed and used[2,30,31], only nitrate (0.1–10 mM) promoted distinct shoot biomass accumulation and root system architecture establishment. Nitrate, but not metabolites, NH_4^+ or Gln that are derived from nitrate assimilation, sustained substantial postembryonic growth (Fig. 1a, c, d and Extended Data Fig. 1a), consistent with uncoupling of nitrate signalling from nitrate metabolism[1,8], NH_4^+ or Gln signalling[2,30,31].

Although nitrate-triggered Ca^{2+} signals could be detected using transgenic aequorin seedlings[22,29], the response was subtle when compared with the flg22-induced Ca^{2+} signals in immune signalling (Extended Data Fig. 1b, c). As nitrate signalling and assimilation occur in both leaves and roots (Extended Data Fig. 1a, d, e), we developed a versatile single-cell system to investigate live Ca^{2+} signalling stimulated by nitrate in mesophyll protoplasts[12,13,23,32]. In leaf cells co-expressing the ultrasensitive Ca^{2+} biosensor GCaMP6 (ref. 33) and a nuclear mCherry, single-cell live recordings revealed that nitrate specifically stimulated a unique and dynamic Ca^{2+} signature in the nucleus and cytosol (Fig. 1e, f). Chelating exogenous Ca^{2+} by EGTA diminished the nitrate-triggered Ca^{2+} signature (Fig. 1f). Unlike the transient and acute cytosolic calcium concentration ($[Ca^{2+}]$cyt) increase stimulated by osmotic and cold stresses in seedlings[22,34], nuclear Ca^{2+} oscillation in symbiosis[35], or a 10-s $[Ca^{2+}]$cyt peak triggered by nitrate in roots[29], a gradually rising subcellular Ca^{2+} signature

Figure 1 | Nitrate triggers unique Ca²⁺-CPK signalling. a, Dual
nitrate functions in plants. **b**, *Arabidopsis* seedling development
without exogenous nitrogen for up to 4 days. Scale bars, 1 mm. Images
are representative of 10 seedlings. **c, d**, Nitrate specifically promotes
extensive shoot and root developmental programs. Different nitrogen
sources (1 mM) were applied at day 5. Error bars denote ± s.e.m., $n = 10$
seedlings. Scale bar, 1 cm. **e**, Time-lapse images of Ca²⁺ signalling in
the nucleus and cytosol stimulated by nitrate in mesophyll protoplasts
expressing GCaMP6. 10 mM KNO₃. BF, bright field. NLS–mC denotes
nuclear HY5–mCherry (a control for protoplast co-transfection and
nuclear localization). Scale bars, 10 μm. Images are representative of
10 protoplasts. **f**, Traces of GCaMP6 signals stimulated by nitrate in
mesophyll protoplasts. 10 mM KNO₃. $(F − F_0)/F_0$ denotes the relative
fluorescence intensity. Error bars (grey areas, 199 error bars) denote s.e.m.,
$n = 10$ protoplasts. **g**, Time-lapse images of Ca²⁺ signalling in mesophyll
cells of cotyledons in GCaMP6 transgenic plants. 10 mM KNO₃. Scale
bars, 50 μm. Images are representative of 10 cotyledons. **h**, Subgroup
III CPKac and nitrate synergistically activate *NIR-LUC* in protoplast
transient assays. *UBQ10-GUS* is a control for protoplast co-transfection
and internal control. 0.5 mM KNO₃, 2 h. Error bars denote s.d., $n = 3$
biological replicates. Dashed line denotes KNO₃ induction without CPKac.
CPKac–Flag expression was determined by immunoblot analyses. Source
Data can be found in the Supplementary Information. **i**, The relation tree
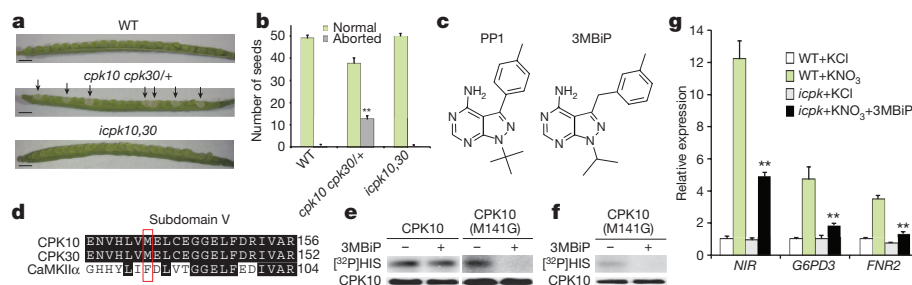of subgroup III CPKs.

attributed to nitrate over a course of minutes was recorded by GCaMP6-
based imaging with high subcellular resolution. Time-lapse recording
using transgenic GCaMP6 plants uncovered a Ca²⁺ signature of simi-
lar amplitude and dynamic stimulated by nitrate in mesophyll cells of
intact plants (Fig. 1g). Distinct Ca²⁺ dynamics were also triggered by
nitrate in the tip, pericycle and stele of intact roots with demonstrated
nitrate signalling activities[7,13,15] (Extended Data Fig. 1f, g). To connect
this distinctive Ca²⁺ signature physiologically (Supplementary Videos
1–4) to established primary nitrate responses, we showed that the acti-
vation of universal nitrate-responsive marker genes *NIR1*, *G6PD3* and
FNR2 was significantly reduced by Gd³⁺ and La³⁺ (blockers of plasma
membrane Ca²⁺ channels) or by W7 (an intracellular Ca²⁺ sensor
inhibitor) (Extended Data Fig. 2a, b) in seedlings[23,28,29]. Our results
support a crucial role for nitrate-induced Ca²⁺ signalling in multiple
cell types of different tissues and organs.

To search for candidates of intracellular Ca²⁺ sensors mediating
primary nitrate signalling, we conducted an in-gel kinase assay
and detected enhanced activity of endogenous CPKs in response
to nitrate within 10 min (Extended Data Fig. 2c). The molecular
mass of nitrate-activated protein kinases was similar to that of most
CPKs but not CIPKs[17–19,23]. There are 34 *Arabidopsis* CPK genes
mediating diverse signalling pathways with complex and redundant
functions[23,24,26,36]. As *cpk* mutants have escaped from mutant screens
for nitrate signalling[7,11], a simple, rapid and reliable cell-based reporter
assay could facilitate targeted functional genomic screening of CPK
candidates involved in nitrate signalling[23]. Using a luciferase (LUC)
reporter gene *NIR-LUC* that exhibits a physiological nitrate response
in transgenic *Arabidopsis* plants[11], we observed rapid, specific and
sensitive regulation of LUC activity by 0.1–50 mM KNO₃ within 2 h
(Extended Data Fig. 2d–f). Unexpectedly, co-expressing *NIR-LUC*
with a constitutively active construct (CPKac)[23] for each of the 25
CPK genes expressed in mesophyll protoplasts did not trigger marked
NIR-LUC activation (Fig. 1h). To test the possibility that the CPKac-
mediated response could be sensitized by low nitrate, we added 0.5 mM
KNO₃ to the protoplast incubation medium. Interestingly, subgroup
III constitutively active CPKs (CPK7ac, CPK8ac, CPK10ac, CPK13ac,
CPK30ac and CPK32ac) were most effective at synergistically activat-
ing *NIR-LUC* together with 0.5 mM KNO₃ (Fig. 1h, i and Extended
Data Fig. 2g). Although specific CPKac is sufficient to activate stress or
immune responses associated with strong and distinct Ca²⁺ signalling
patterns[22–24,26,34], activation of subgroup III CPKac alone did not fully
evoke specific nitrate response. Consistent with our findings, it has
been suggested that primary nitrate signalling requires the coordination
of multiple signalling mechanisms[2,6,12,13,18,37]. Our results indicate that
nitrate may specify and synergize functionally redundant subgroup III
CPKs in *NIR-LUC* activation.

Chemical switch defines CPK signalling

To test the specificity and physiological roles of subgroup III CPKs, we
examined loss-of-function *cpk* mutants. The single *cpk7*, *cpk8*, *cpk10*,
cpk13, *cpk30* or *cpk32* mutants barely affected nitrate-responsive genes
and lacked overt growth phenotypes (Extended Data Fig. 3a–g). As
CPK10 and CPK30 share the highest sequence identity and slight
modulation of *NIR* and *G6PD3* expression (Fig. 1i and Extended Data
Figs 2g, 3d), we attempted to generate the *cpk10 cpk30* double mutant.
However, analyses of the siliques revealed that the *cpk10 cpk30* double
mutant was lethal at early embryogenesis (Fig. 2a, b).

Aiming to simultaneously overcome embryo lethality and enable
analyses of higher-order *cpk* mutants, we engineered CPK10 to be
reversibly inhibited by 3MBiP (1-isopropyl-3-(3-methylbenzyl)-
1*H*-pyrazolo[3,4-*d*]pyrimidin-4-amine), a specific and improved
derivative of the protein kinase inhibitor PP1 (4-amino-5-(methylphe-
nyl)-7-(*t*-butyl)pyrazolo-(3,4-*d*)pyrimidine)[38,39] (Fig. 2c). A critical
determinant of protein kinase inhibitor selectivity is the size of the
gatekeeper residue in the ATP-binding pocket[38,39]. By aligning the
conserved protein kinase subdomain V in *Arabidopsis* CPK10, CPK30
and human CaMKIIα, we created the CPK10(M141G) gatekeeper
residue mutant (Fig. 2d). Notably, 3MBiP completely inhibited the
kinase activity of CPK10(M141G) but not wild-type CPK10 (Fig. 2e).
A genomic construct expressing CPK10(M141G) was introduced into
cpk10 cpk30/+ to rescue the lethal embryo phenotype of its *cpk10 cpk30*
progenies, creating a 3MBiP-inducible *icpk10,30* mutant (Fig. 2a, b).
The haemagglutinin (HA)-tagged CPK10(M141G) protein immu-
noprecipitated from the transgenic plants was completely inhibited
by 3MBiP (Fig. 2f). Because CPK32ac greatly enhanced *NIR-LUC*
expression (Fig. 1h), we also generated *cpk10 cpk32* and *cpk30 cpk32*
double mutants, as well as a 3MBiP-inducible *icpk10,30,32* triple
mutant expressing CPK10(M141G)–HA (designated *icpk*) by genetic
crosses and molecular confirmation. Nitrate-responsive marker genes
were reduced in double mutants, such as *cpk10 cpk32*, *cpk30 cpk32*
and *icpk10,30*, in the presence of 3MBiP (Extended Data Fig. 3i, j),

Figure 2 | Chemical genetic analyses of CPK10, CPK30 and CPK32.
a, **b**, The embryo lethality of *cpk10 cpk30* is rescued by CPK10(M141G) in *icpk10,30*. Arrows indicate aborted embryos. WT, wild type (Col-0). Scale bars, 1 mm. Error bars denote s.d., $n = 10$ siliques. **$P < 0.0001$ (chi-squared test). **c**, Chemical structure of 3MBiP derived from PP1. **d**, The gatekeeper residue in CPK10, CPK30 and human CaMKIIα. **e**, **f**, The CPK10(M141G) activity isolated from protoplasts (**e**) or

icpk10,30 seedlings (**f**) is specifically inhibited by 3MBiP. [^{32}P]HIS, histone phosphorylation. **g**, Nitrate response is significantly diminished in the *icpk* triple mutant seedlings. Error bars, s.d., $n = 3$ biological replicates. *$P < 0.05$, **$P < 0.0001$ (two-way ANOVA with Tukey's multiple comparisons test). Source Data can be found in the Supplementary Information.

without displaying a visible phenotype in plant growth supported by nitrate (Extended Data Fig. 3d, e, g). Expression of nitrate marker genes was further reduced in the 3MBiP-inducible *icpk* triple mutant (Fig. 2g), correlating with retarded plant growth (Extended Data Fig. 3h). Insensitivity of wild-type plants to 3MBiP treatment in gene expression and seedling growth (Fig. 2g and Extended Data Fig. 3e, f, h, j) validated the specificity of 3MBiP. By overcoming dual genetic redundancy and embryo lethality, chemical genetics offers a new approach to determine the dynamic and physiological functions of higher-order *cpk* mutants that was not previously possible.

Nitrate–CPKs control primary transcription
To explore the genome-wide transcriptional landscape controlled by nitrate–CPK signalling, we conducted RNA sequencing (RNA-seq) experiments 15 min after nitrate induction in wild-type and *icpk* seedlings. In wild-type seedlings, 394 and 79 genes were activated and repressed, respectively, in response to nitrate ($\log_2 \geq 1$ or ≤ -1; $q \leq 0.05$), which significantly overlapped with nitrate-responsive genes discovered in microarray-based studies of both roots and shoots[4,8,10,13]. In *icpk*, 266 upregulated (68%) and 44 downregulated (56%) genes could be defined as statistically significant nitrate–CPK target genes (*icpk* KNO$_3$ versus wild-type KNO$_3$, $q \leq 0.05$) (Fig. 3, Extended Data Figs 4, 5 and Supplementary Tables 1 and 2). Thus, CPK10, CPK30 and CPK32 have a central role in regulating primary nitrate responses in the entire plant system.
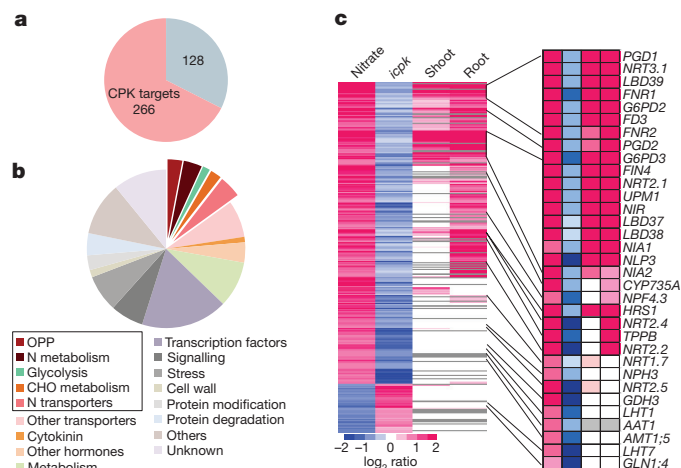
Among the statistically significant primary nitrate–CPK target genes, CPK10, CPK30 and CPK32 modulated diverse key cellular and metabolic functions immediately activated by nitrate[1–5,8,10,12,13,21]. The most significantly enriched functional classes of genes were those supporting nitrate transport and assimilation; two routes of glucose-6-phosphate metabolism via the oxidative pentose-phosphate pathway and glycolysis; amino acid transport and metabolism; other transporters; carbon/nitrogen metabolism; cytokinin, auxin and abscisic acid metabolism and signalling; protein degradation; stress; signalling; and transcription (Fig. 3b, c, Extended Data Fig. 4 and Supplementary Tables 1 and 2). Notably, the universal nitrate-inducible genes responsible for the conserved nitrogen uptake and assimilation processes from *Arabidopsis*, rice to maize were regulated by the CPK10, CPK30 and CPK32 protein kinases[1,3–5,12,13,16,28] (Extended Data Fig. 4e–g). Nearly 50 genes encoding annotated transcription factors were activated by nitrate via CPK10, CPK30 and CPK32 (Supplementary Table 2), providing potential amplification of the downstream nitrate transcriptional network[12,13,15,20,21]. Nitrate–CPK signalling repressed genes were involved in transcription, metabolism and transport (Extended Data Fig. 4b, d and Supplementary Table 2).

We carried out quantitative PCR with reverse transcription (RT–qPCR) analyses of primary nitrate–CPK target genes for eight major functional classes, including the oxidative pentose-phosphate

pathway, nitrate and amino acid transporters, nitrogen metabolism, carbohydrate metabolism, signalling, cytokinin synthesis, and transcription factors in wild-type and *icpk* mutant plants (Extended Data Fig. 4f, g and Supplementary Table 2). Notably, nitrate activation of *CYP735A2* expression to enhance *trans*-zeatin synthesis is crucial for shoot development, providing an interconnection between local and systemic nitrate signalling via the action of a mobile growth hormone[40]. As nitrate activation of these marker genes was markedly diminished in the *icpk* mutant, CPK10, CPK30 and CPK32 are master regulators in primary nitrate signalling and integrate global gene expression to nitrate-activated metabolic and physiological responses (Fig. 3, Extended Data Fig. 4e–g and Supplementary Table 2).
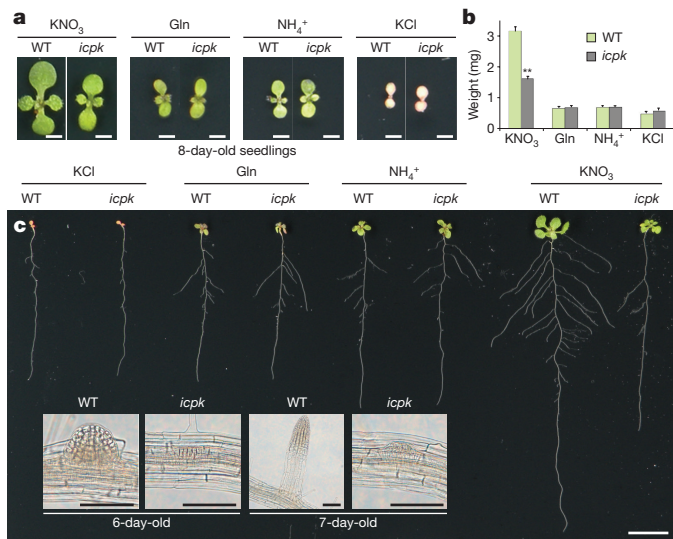
Nitrate–CPKs dictate growth plasticity
To investigate the nexus between nitrate-specific developmental programs (Fig. 1c, d) and nitrate–CPK signalling, we examined shoot growth by quantifying shoot fresh weight in wild-type and *icpk* seedlings. To bypass any early effect of nitrate on seed germination, we selected 3-day-old seedlings without apparent phenotypes on ammonium plates and placed them on 3MBiP medium in the presence of

Figure 3 | CPK10, CPK30 and CPK32 control primary nitrate-responsive transcriptome. Transcriptome analyses of the primary nitrate response in wild-type and *icpk* seedlings by RNA-seq. **a**, Nitrate–CPK-upregulated target genes. Red, genes significantly affected in *icpk* ($q \leq 0.05$). **b**, MapMan functional categories for nitrate–CPK-upregulated target genes. **c**, Hierarchical clustering analysis of nitrate–CPK target genes. Nitrate denotes primary nitrate-responsive genes in the wild-type seedlings; *icpk* denotes nitrate–CPK target genes. Shoot or root denote nitrate-responsive genes identified by ATH1 gene chips in shoots or roots, repsectively[4]. Grey denotes gene probes not present on the ATH1 gene chip.
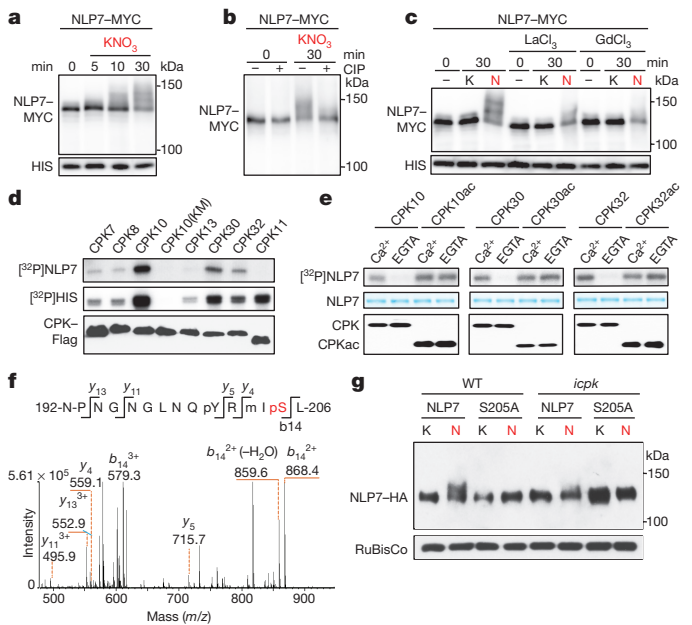
Figure 4 | Dynamic Nitrate–CPK signalling orchestrates development of shoots and roots. a, b, The *icpk* mutant exhibits deficiency in nitrate-specific promotion of shoot development. Different nitrogen sources (5 mM KNO_3, 2.5 mM ammonium succinate (NH_4^+), 5 mM KCl or 1 mM Gln) and 1 μM 3MBiP were applied after 3 days on 2.5 mM ammonium succinate to ensure even germination. Scale bars, 0.5 cm. Error bars, s.e.m., $n = 17$ seedlings. $**P < 0.0001$ (two-way ANOVA with Tukey's multiple comparisons test). **c,** The root system architecture defects of *icpk* are nitrate specific. Scale bar, 1 cm. Insets, the third lateral root development induced by nitrate for 3 days (6-day-old) or 4 days (7-day-old) in wild-type and *icpk* seedlings. Scale bars, 100 μm. Images are representative of 10 seedlings.

Figure 5 | The CPK–NLP signalling connection. a, b, Nitrate triggers a phosphorylation-dependent mobility shift of NLP7 in transgenic seedlings. 10 mM KNO_3. CIP, calf-intestinal alkaline phosphatase. **c,** Ca^{2+} channel blockers diminish nitrate-triggered NLP7 phosphorylation. 10 mM KCl (K) or KNO_3 (N). **d,** CPK10, CPK30 and CPK32 phosphorylate NLP7 *in vitro*. **e,** Phosphorylation of NLP7 by CPK10, CPK30 and CPK32 is Ca^{2+}-dependent. **f,** Mass spectrometric analysis of NLP7 phosphorylation at Ser205. **g,** Nitrate-induced phosphorylation of NLP7 at Ser205 is abolished in *icpk*. 10 mM KCl or KNO_3 for 15 min.

KCl, NH_4^+, Gln or KNO_3 for 5–8 days. Although NH_4^+ or Gln could promote limited shoot greening and growth equally in wild-type and *icpk* seedlings, nitrate was essential for full greening and expansion of cotyledons and true leaves in wild-type seedlings[5,11] (Fig. 4 and Extended Data Figs 1a, 6a). The specific *icpk* deficiency of cotyledon and leaf expansion in response to nitrate (Fig. 4a–c) might be partially correlated with reduced expression of *CYP735A2* for *trans*-zeatin synthesis[40] (Extended Data Fig. 4f, g).

We next examined the roles of CPK10, CPK30 and CPK32 in nitrate-specific control of the root developmental program. The nitrate-specific stimulation of lateral root primordia density was reduced and lateral root elongation was severely retarded in *icpk* (Fig. 4c and Extended Data Fig. 6). Although ammonium supported lateral root initiation similarly in wild-type and *icpk* seedlings[2,31], nitrate–CPK signalling was essential for lateral root primordia progression and emergence, as well as lateral root elongation (Fig. 4c and Extended Data Fig. 6c–e). We quantified the dynamic distribution of all lateral roots from primordia stages I–VII to emergence (Em) and fully elongated (LR) stages[41] in wild-type and *icpk* seedlings. The proportion of emerged lateral root (Em + LR) increased from 0% (4 days) to 40% (8 days) after transfer to the nitrate medium, and 3MBiP did not affect the normal development of root systems in the wild-type seedlings. By contrast, the *icpk* lateral root primordia were arrested most conspicuously in roots 6–8 days after transfer (Extended Data Fig. 6d–g).

Notably, the primary root length was similar between the wild-type and *icpk* 8-day-old seedlings on KCl or on different nitrogen media. Thus, the growth of primary roots at the early stage of development immediately after germination relied mainly on the seed nutrient reserves and sugars, with limited influence by exogenous nitrogen nutrients[32,42] (Extended Data Fig. 6a, b). The 11-day-old wild-type and *icpk* plants were indistinguishable on KCl, NH_4^+ or Gln medium, displaying limited shoot and root growth and development. However, vigorous primary and lateral root growth promoted by exogenous nitrate was abolished in *icpk* (Figs 1c, d and 4c)[11]. CPK10, CPK30 and
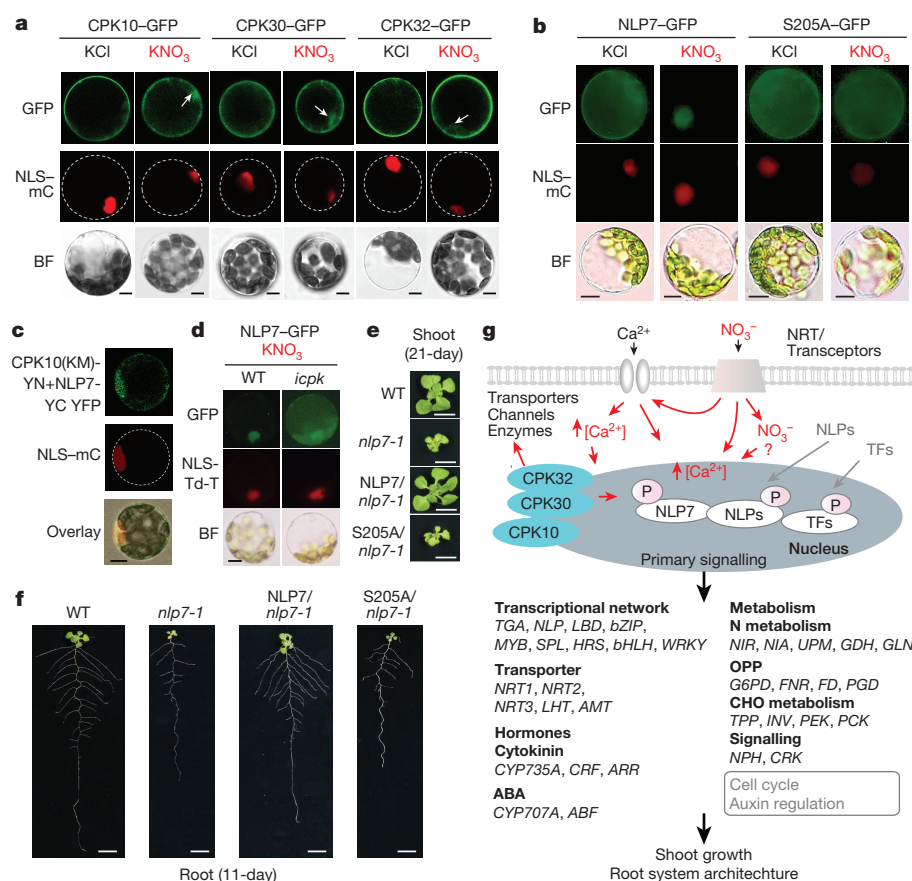
CPK32 specifically defined the long-term systemic shoot developmental program and root system architecture via modulating the primary nitrate-signalling network[2,11].

The nitrate–CPK–NLP regulatory network

Arabidopsis NLP6 and NLP7 have been identified as key transcription factors of primary nitrate responses, but how they are activated by nitrate remains unknown[2,3,8,9,12,13,21]. Analyses of transgenic plants revealed a nitrate-stimulated NLP6–MYC and NLP7–MYC mobility shift at 5–30 min, which was eliminated by phosphatase (Fig. 5a, b and Extended Data Fig. 7a, b). The nitrate-stimulated NLP7–MYC phosphorylation was greatly diminished by Gd^{3+} and La^{3+} (Fig. 5c), or by W7 (Extended Data Fig. 7c), analogous to the nitrate-responsive gene regulation (Extended Data Fig. 2a, b). Furthermore, CPK10, CPK30 and CPK32, but not the kinase-dead mutant CPK10(KM) or the subgroup I CPK11, phosphorylated NLP7 *in vitro* (Fig. 5d). As the Ca^{2+} chelator EGTA abolished the phosphorylation of NLP7 or histone by CPK10, CPK30 and CPK32 but not by CPK10ac, CPK30ac and CPK32ac lacking the Ca^{2+}-binding domain[23–26] (Fig. 5e and Extended Data Fig. 7d), CPK10, CPK30 and CPK32 were Ca^{2+} sensors and effectors to relay nitrate signalling. The nitrate–CPK–NLP6/NLP7 signalling link was further supported by the considerable overlaps between nitrate–CPK and nitrate–NLP6/NLP7 target genes as universal nitrate response marker genes[3,12,13] (Fig. 3c, Extended Data Figs 4, 5 and Supplementary Table 2).

By aligning nine *Arabidopsis* NLPs and four orthologous *Lotus japonicus* NLPs using integrated computational and literature analyses[3,12,13], we identified a uniquely conserved serine (Ser205 in NLP7) as a candidate CPK phosphorylation site (Extended Data Fig. 7e). CPK10ac, CPK30ac and CPK32ac phosphorylated the nitrate-responsive domain of wild-type NLP7-N(1–581 amino acids)[12] but not NLP7-N(S205A) (Extended Data Fig. 7f). Moreover, NLP7(S205A) lost nitrate-stimulated phosphorylation in transgenic

Figure 6 | Nitrate–CPK–NLP signalling is crucial in nutrient–growth networks. a, CPK10, CPK30 and CPK32 translocate to the nucleus in response to nitrate. 10 mM KNO_3. Scale bars, 10 μm. Images are representative of 8 protoplasts. BF, bright field. NLS–mC denotes nuclear HY5–mCherry. **b**, Phosphorylation of Ser205 is required for nitrate-triggered nuclear retention of NLP7–GFP. 10 mM KNO_3. Scale bars, 10 μm. Images are representative of 10 protoplasts. **c**, CPK10(KM) interacts with NLP7 in the nucleus in the BiFC assay. 10 mM KNO_3. Images are representative of 8 protoplasts. **d**, Nitrate-triggered nuclear retention of NLP7–GFP is diminished in *icpk*. 10 mM KNO_3. NLS-Td-T denotes nuclear Td-Tomato (a control for protoplast co-transfection and nuclear localization). Images are representative of 8 protoplasts. **e, f**, NLP7–GFP but not NLP7(S205A)–GFP complements the *nlp7* mutant. Scale bars, 1 cm. Images are representative of 20 seedlings. **g**, Nitrate–CPK–NLP signalling model. TFs, transcription factors.

plants (Extended Data Fig. 7g). Mass spectrometry analyses confirmed that Ser205 in NLP7 was phosphorylated *in vivo* in the presence of nitrate (Fig. 5f). Like CPK10ac, CPK30ac and CPK32ac, NLP7 over-expression but neither kinase-dead CPK10ac(KM) nor NLP7(S205A), acted synergistically with 0.5 mM nitrate to enhance *NIR-LUC* activation (Fig. 1h and Extended Data Fig. 7h). Finally, nitrate-triggered NLP7 phosphorylation at Ser205 *in vivo* was abolished in the *icpk* mutant (Fig. 5g).

To validate the nitrate–CPK–NLP link further, we discovered nitrate-stimulated rapid nuclear translocation of green fluorescent protein (GFP)-tagged CPK10, CPK30 and CPK32 by confocal imaging (Fig. 6a and Extended Data Fig. 8a). NLP7–GFP but not NLP7(S205A)–GFP responded to nitrate stimulation with persistent nuclear localization in leaf cells (Fig. 6b) and in the transgenic *nlp7* roots[13] (Extended Data Fig. 8b). Using an *in vivo* bimolecular fluorescence complementation (BiFC) assay, we showed that CPK10(KM) directly interacted with NLP7 in the nucleus in the presence of nitrate in protoplasts (Fig. 6c). Nitrate-stimulated nuclear retention of NLP7–GFP was greatly diminished in *icpk* protoplasts (Fig. 6d). These complementary *in vivo* and *in vitro* analyses provided compelling evidence to support the signalling connections from CPK10, CPK30 and CPK32 to NLP phosphorylation in mediating primary nitrate signalling and transcription.

To identify functionally important NLP7 target genes in the nitrate–CPK–NLP signalling network, we explored genome-wide transcriptional profiling in the nitrate-responsive transient transactivation system[3,12,13]. We discovered that NLP7–HA but not NLP7(S205A)–HA could robustly activate a wide range of putative NLP7 target genes in mesophyll cells[3,4,12,13,28] (Extended Data Fig. 9a–c and Supplementary Tables 1 and 2). Notably, NLP7 could also target and ectopically activate *NRT2.1* and *TPPB*, which are normally silenced in mesophyll cells but are nitrate-inducible in root cells (Fig. 3, Extended Data Fig. 9a, c). Our results are consistent with the activation of *NRT2.1-LUC*,

NRE-LUC or *NIR-LUC* by ectopic NLP1, NLP2, NLP5, NLP6, NLP7 and NLP9 expression[12,13], the repression of primary nitrate-responsive marker genes in dominant-negative NLP6 (NLP6-SUPRD) transgenic plants[3,12], as well as chromatin immunoprecipitation with DNA microarray (ChIP–chip) analyses of NLP7–GFP after 10-min nitrate treatment in transgenic seedlings[13]. Notably, we also identified potential NLP7 target genes for cell cycle initiation and auxin hormone regulators (Extended Data Fig. 9b, c). Future research will aim to determine the functions of specific NLP7 target genes in various plant organs and cell types. The identification of new NLP7 target genes was supported by the unique *nlp7* phenotypes and the complementation of *nlp7* by NLP7–GFP but not NLP7(S205A)–GFP for proliferation and growth in shoots and roots (Fig. 6e, f and Extended Data Fig. 10). The broad spectrum of nitrate-associated mutant phenotypes and primary nitrate-responsive-transcriptome defects were shared by *icpk* and *nlp7* (refs 9, 13). As the specific serine residue is conserved among *Arabidopsis* and *L. japonicus* NLPs (Extended Data Fig. 7e), CPK10, CPK30 and CPK32 could potentially phosphorylate and activate all NLPs and possibly other transcription factors with overlapping or distinct target genes to support transcriptional, metabolic and system-wide nutrient–growth regulations differentially manifested in wild-type and conditional *icpk* mutant plants[2,3,9,12,13,21] (Figs 2g, 3–6 and Extended Data Figs 3–10).

Discussion

We have uncovered a nitrate-coupled Ca^{2+} signalling mechanism central to the plant nutrient–growth regulatory network using multifaceted approaches, encompassing an ultrasensitive Ca^{2+} biosensor, a sensitized and targeted functional genomic screen, a chemical switch for conditional higher-order *Arabidopsis cpk* mutants, as well as integrated cellular, biochemical, genetic and systems analyses. Our findings connected a new Ca^{2+}–CPK–NLP signalling cascade to comprehensive nitrate responses and revealed a previously unrecognized

function of Ca^{2+}-sensor CPKs as master regulators that orchestrate nitrate-activated signalling (Fig. 6g). As CPKs and NLPs are evolutionarily conserved from algae to land plants[3,9,12,13,24–26], the nitrate–CPK–NLP signalling relay may be widespread in the plant kingdom. Our discoveries expand the biological functions of Ca^{2+} signalling to nutrient responses essential to all life forms. Future progress is likely to identify sensors, channels and other regulators involved in generating complex Ca^{2+} signatures in plant responses to nitrate, other nutrients, peptides, hormones and environmental cues that capitalize on continued advances of ultrasensitive Ca^{2+} biosensors[33]. This work provides a molecular framework for future research on the complex interactions between nitrogen and sugar signalling pathways central to all aspects of nutrient-mediated growth regulation in plants and animals[1,2,4,5,32,42–44].

1. Nunes-Nesi, A., Fernie, A. R. & Stitt, M. Metabolic and signaling aspects underpinning the regulation of plant carbon nitrogen interactions. *Mol. Plant* **3**, 973–996 (2010).
2. Kiba, T. & Krapp, A. Plant nitrogen acquisition under low availability: regulation of uptake and root architecture. *Plant Cell Physiol.* **57**, 707–714 (2016).
3. Konishi, M. & Yanagisawa, S. Emergence of a new step towards understanding the molecular mechanisms underlying nitrate-regulated gene expression. *J. Exp. Bot.* **65**, 5589–5600 (2014).
4. Wang, R., Okamoto, M., Xing, X. & Crawford, N. M. Microarray analysis of the nitrate response in *Arabidopsis* roots and shoots reveals over 1,000 rapidly responding genes and new linkages to glucose, trehalose-6-phosphate, iron, and sulfate metabolism. *Plant Physiol.* **132**, 556–567 (2003).
5. Scheible, W. R. *et al.* Genome-wide reprogramming of primary and secondary metabolism, protein synthesis, cellular growth processes, and the regulatory infrastructure of *Arabidopsis* in response to nitrogen. *Plant Physiol.* **136**, 2483–2499 (2004).
6. Bouguyon, E. *et al.* Multiple mechanisms of nitrate sensing by *Arabidopsis* nitrate transceptor NRT1.1. *Nature Plants* **1**, 15015 (2015).
7. Wang, R., Xing, X., Wang, Y., Tran, A. & Crawford, N. M. A genetic screen for nitrate regulatory mutants captures the nitrate transporter gene NRT1.1. *Plant Physiol.* **151**, 472–478 (2009).
8. Wang, R. *et al.* Genomic analysis of the nitrate response using a nitrate reductase-null mutant of *Arabidopsis*. *Plant Physiol.* **136**, 2512–2522 (2004).
9. Castaings, L. *et al.* The nodule inception-like protein 7 modulates nitrate sensing and metabolism in *Arabidopsis*. *Plant J.* **57**, 426–435 (2009).
10. Krouk, G., Mirowski, P., LeCun, Y., Shasha, D. E. & Coruzzi, G. M. Predictive network modeling of the high-resolution dynamic plant transcriptome in response to nitrate. *Genome Biol.* **11**, R123 (2010).
11. Liu, K. H., McCormack, M. & Sheen, J. Targeted parallel sequencing of large genetically-defined genomic regions for identifying mutations in *Arabidopsis*. *Plant Methods* **8**, 12 (2012).
12. Konishi, M. & Yanagisawa, S. *Arabidopsis* NIN-like transcription factors have a central role in nitrate signalling. *Nat. Commun.* **4**, 1617 (2013).
13. Marchive, C. *et al.* Nuclear retention of the transcription factor NLP7 orchestrates the early response to nitrate in plants. *Nat. Commun.* **4**, 1713 (2013).
14. Guan, P. *et al.* Nitrate foraging by *Arabidopsis* roots is mediated by the transcription factor TCP20 through the systemic signaling pathway. *Proc. Natl Acad. Sci. USA* **111**, 15267–15272 (2014).
15. Alvarez, J. M. *et al.* Systems approach identifies TGA1 and TGA4 transcription factors as important regulatory components of the nitrate response of *Arabidopsis thaliana* roots. *Plant J.* **80**, 1–13 (2014).
16. Obertello, M., Shrivastava, S., Katari, M. S. & Coruzzi, G. M. Cross-species network analysis uncovers conserved nitrogen-regulated network modules in rice. *Plant Physiol.* **168**, 1830–1843 (2015).
17. Hu, H. C., Wang, Y. Y. & Tsay, Y. F. AtCIPK8, a CBL-interacting protein kinase, regulates the low-affinity phase of the primary nitrate response. *Plant J.* **57**, 264–278 (2009).
18. Ho, C. H., Lin, S. H., Hu, H. C. & Tsay, Y. F. CHL1 functions as a nitrate sensor in plants. *Cell* **138**, 1184–1194 (2009).
19. Léran, S. *et al.* Nitrate sensing and uptake in *Arabidopsis* are enhanced by ABI2, a phosphatase inactivated by the stress hormone abscisic acid. *Sci. Signal.* **8**, ra43 (2015).
20. Medici, A. *et al.* AtNIGT1/HRS1 integrates nitrate and phosphate signals at the *Arabidopsis* root tip. *Nat. Commun.* **6**, 6274 (2015).
21. Vidal, E. A., Álvarez, J. M., Moyano, T. C. & Gutiérrez, R. A. Transcriptional networks in the nitrate response of *Arabidopsis thaliana*. *Curr. Opin. Plant Biol.* **27**, 125–132 (2015).
22. Knight, H., Trewavas, A. J. & Knight, M. R. Cold calcium signaling in *Arabidopsis* involves two cellular pools and a change in calcium signature after acclimation. *Plant Cell* **8**, 489–503 (1996).
23. Boudsocq, M. *et al.* Differential innate immune signalling via Ca^{2+} sensor protein kinases. *Nature* **464**, 418–422 (2010).
24. Boudsocq, M. & Sheen, J. CDPKs in immune and stress signaling. *Trends Plant Sci.* **18**, 30–40 (2013).
25. Reddy, A. S., Ali, G. S., Celesnik, H. & Day, I. S. Coping with stresses: roles of calcium- and calcium/calmodulin-regulated gene expression. *Plant Cell* **23**, 2010–2032 (2011).
26. Simeunovic, A., Mair, A., Wurzinger, B. & Teige, M. Know where your clients are: subcellular localization and targets of calcium-dependent protein kinases. *J. Exp. Bot.* **67**, 3855–3872 (2016).
27. Ebert, D. H. & Greenberg, M. E. Activity-dependent neuronal signalling and autism spectrum disorder. *Nature* **493**, 327–337 (2013).
28. Sakakibara, H., Kobayashi, K., Deji, A. & Sugiyama, T. Partial characterization of the signaling pathway for the nitrate-dependent expression of genes for nitrogen-assimilatory enzymes using detached maize leaves. *Plant Cell Physiol.* **38**, 837–843 (1997).
29. Riveras, E. *et al.* The calcium ion is a second messenger in the nitrate signaling pathway of *Arabidopsis*. *Plant Physiol.* **169**, 1397–1404 (2015).
30. Forde, B. G. Glutamate signalling in roots. *J. Exp. Bot.* **65**, 779–787 (2014).
31. Giehl, R. F., Gruber, B. D. & von Wirén, N. It's time to make changes: modulation of root system architecture by nutrient signals. *J. Exp. Bot.* **65**, 769–778 (2014).
32. Xiong, Y. *et al.* Glucose-TOR signalling reprograms the transcriptome and activates meristems. *Nature* **496**, 181–186 (2013).
33. Chen, T. W. *et al.* Ultrasensitive fluorescent proteins for imaging neuronal activity. *Nature* **499**, 295–300 (2013).
34. Yuan, F. *et al.* OSCA1 mediates osmotic-stress-evoked Ca^{2+} increases vital for osmosensing in *Arabidopsis*. *Nature* **514**, 367–371 (2014).
35. Charpentier, M. *et al.* Nuclear-localized cyclic nucleotide-gated channels mediate symbiotic calcium oscillations. *Science* **352**, 1102–1105 (2016).
36. Brandt, B. *et al.* Calcium specificity signaling mechanisms in abscisic acid signal transduction in *Arabidopsis* guard cells. *eLife* **4**, e03599 (2015).
37. Gan, Y., Bernreiter, A., Filleur, S., Abram, B. & Forde, B. G. Overexpressing the ANR1 MADS-box gene in transgenic plants provides new insights into its role in the nitrate regulation of root development. *Plant Cell Physiol.* **53**, 1003–1016 (2012).
38. Liu, Y. *et al.* Structural basis for selective inhibition of Src family kinases by PP1. *Chem. Biol.* **6**, 671–678 (1999).
39. Zhang, C. *et al.* Structure-guided inhibitor design expands the scope of analog-sensitive kinase technology. *ACS Chem. Biol.* **8**, 1931–1938 (2013).
40. Kiba, T., Takei, K., Kojima, M. & Sakakibara, H. Side-chain modification of cytokinins controls shoot growth in *Arabidopsis*. *Dev. Cell* **27**, 452–461 (2013).
41. Malamy, J. E. & Benfey, P. N. Organization and cell differentiation in lateral roots of *Arabidopsis thaliana*. *Development* **124**, 33–44 (1997).
42. Sheen, J. Master regulators in plant glucose signaling networks. *J. Plant Biol.* **57**, 67–79 (2014).
43. Efeyan, A., Comb, W. C. & Sabatini, D. M. Nutrient-sensing mechanisms and pathways. *Nature* **517**, 302–310 (2015).
44. Rebsamen, M. *et al.* SLC38A9 is a component of the lysosomal amino acid sensing machinery that controls mTORC1. *Nature* **519**, 477–481 (2015).

Author Contributions K.L., Y.N., J.S. and S.Y. conceived and initiated the project, and designed the experiments. K.L., Y.N., M.K., Y.W., H.D., H.S.C., L.L., M.B. and J.S. performed experiments. M.M., Y.N. and H.S.C. performed bioinformatics. S.M. and T.I. conducted LC–MS/MS analysis. C.Z. and K.S. provided 3MBiP and suggestions. J.S., K.L., Y.N. and S.Y. wrote the manuscript. All authors discussed the results and commented on the manuscript.

Author Information Reprints and permissions information is available at www.nature.com/reprints. The authors declare no competing financial interests. Readers are welcome to comment on the online version of the paper. Publisher's note: Springer Nature remains neutral with regard to jurisdictional claims in published maps and institutional affiliations. Correspondence and requests for materials should be addressed to K.L. (khliu@molbio.mgh.harvard.edu), S.Y. (asyanagi@mail.ecc.u-tokyo.ac.jp) or J.S. (sheen@molbio.mgh.harvard.edu).

Reviewer Information *Nature* thanks H. Sakakibara and the other anonymous reviewer(s) for their contribution to the peer review of this work.

METHODS

Plasmid constructs and transgenic lines. The 1.3-kb GCaMP6 coding region was PCR amplified from the pGP-CMV-GCaMP6s plasmid (Addgene)[33]. The amplified DNA was then inserted into the plant expression vector (the HBT-HA-NOS plasmid)[45] to generate the HBT-GCaMP6-HA construct. The HBT-GCaMP6-HA construct was inserted into the binary vector pCB302 (ref. 46) to generate the HBT-GCaMP6-HA transgenic plants using the *Agrobacterium* (GV3101)-mediated floral-dip method[47]. Transgenic plants were selected by spraying with the herbicide BASTA. The construct expressing HY5–mCherry was used as a control for protoplast co-transfection and nucleus labelling, and was obtained from J.-G. Chen[48]. NLS-Td-Tomato was used as a control for protoplast co-transfection and nucleus labelling, and was obtained from X. Liu. *NIR-LUC* was constructed as described previously[11]. *UBQ10-GUS* is a control for protoplast co-transfection and internal control; all HBT-CPKac-Flag-NOS expression plasmids have been described previously[23]. To construct HBT-CPK-GFP-NOS, the coding regions of the *CPK10*, *CPK30* and *CPK32* cDNA were amplified and then cloned into the HBT-GFP-NOS plasmid[23]. HBT-CPK10(M141G)-Flag was generated by site-directed mutagenesis of the HBT-CPK10-Flag construct. To complement the *cpk10 cpk30/+* mutant, a 5.5-kb DNA fragment including the promoter region (3 kb) and the coding region of *CPK10* was amplified from genomic DNA, which was then cloned into the plasmid HBT-HA-NOS and mutagenized to generate pCPK10-CPK10(M141G)-HA-NOS. The pCPK10-CPK10(M141G)-HA-NOS construct was inserted into pCB302 and transformed into *cpk10 cpk30/+* mutant plants using the *Agrobacterium* (GV3101)-mediated floral-dip method[47]. At the T3 generation, homozygous single-copy insertion lines were screened for the *cpk10 cpk30* double mutant carrying pCPK10-CPK10(M141G)-HA-NOS to obtain the 3MBiP-inducible icpk10,30 double mutant, which rescued the embryo lethality of the *cpk10 cpk30* double mutant. The 3MBiP-inducible icpk10,30,32 triple mutant expressing CPK10(M141G)-HA (designated icpk) was generated by genetic cross to *cpk32* and confirmed by molecular analyses. To construct 35SΩ-NLP6-MYC or 35SΩ-NLP7-MYC in the pCB302 binary plasmid with hygromycin B selection, the β-glucuronidase (*GUS*) gene in the 35SΩ-GUS plasmid[49] was replaced with the DNA fragment encoding the full-length *NLP6* or *NLP7* fused to 6 copies of the *MYC* epitope tag in the HBT-NLP6-MYC or HBT-NLP7-MYC plasmid[12]. The *NLP6-MYC* and *NLP7-MYC* transgenic plants were generated by *Agrobacterium* (GV3101)-mediated transformation by floral dip and hygromycin B resistance selection. To construct HBT-NLP7-HA and HBT-NLP7-GFP, the 2.9 kb coding region of the *NLP7* cDNA was amplified and then cloned into the HBT-NOS plasmid. HBT-NLP7(S205A)-HA and HBT-NLP7(S205A)-GFP were generated by site-directed mutagenesis. A 7.9-kb genomic DNA fragment of *NLP7* was cloned into the pUC plasmid and fused with GFP at the C terminus to generate pNLP7-NLP7-GFP. The pNLP7-NLP7(S205A)-GFP construct was generated by site-directed mutagenesis. pNLP7-NLP7-GFP or pNLP7-NLP7(S205A)-GFP was then inserted into pCB302 and introduced into *nlp7-1* mutant plants using the *Agrobacterium* (GV3101)-mediated floral-dip[47] method for complementation analyses. To construct UBQ10-CPK10KM-YN and UBQ10-NLP7-YC, the coding regions of CPK10(KM), NLP7, YFP-N terminus and YFP-C terminus were amplified by PCR and cloned into the UBQ10-GUS plasmid. To construct pET14-NLP7-N(1-581)-HIS and pET14-NLP7-N(S205A)-HIS for protein expression, the N-terminal coding region of NLP7 and NLP7(S205A) were amplified from HBT-NLP7-HA and HBT-NLP7(S205A)-HA. All constructs were verified by sequencing. The primers used for plasmid construction and site-directed mutagenesis are listed in Supplementary Table 3.

Plant materials and growth conditions. *Arabidopsis* ecotype Columbia (Col-0) was used as the wild type. The *cpk* mutants were obtained from *Arabidopsis* Biological Resource Centre (ABRC)[50]. Homozygous T-DNA lines were identified using *CPK* gene-specific primers and T-DNA left-border primers. The gene-specific primers used are listed in the Supplementary Table 4. Double mutants were obtained by genetic crosses between *cpk10-1*, *cpk30-1* and *cpk32-1*, and confirmed by PCR. For RT–PCR analysis of *cpk* single mutants, around 30 plants were grown on the Petri dish (150 mm × 15 mm) containing 100 ml of 1/2 × MS medium salt, 0.1% MES, 0.5% sucrose, 0.7% phytoagar under constant light (150 μmol m^{-2} s^{-1}) at 23 °C for 7 days. Samples were collected for RT–PCR analysis. To generate icpk, *cpk32-1* was crossed to icpk10,30. F2 plants were first screened for resistance to BASTA and then confirmed by genotyping (primers listed in Supplementary Table 4) for the homozygous *cpk10 cpk30 cpk32* triple mutants. The homozygous icpk plants were isolated with no segregation for BASTA resistance in F3 plants. To demonstrate embryo lethality in *cpk10 cpk30* mutants, *cpk10 cpk30/+* plants were grown at a photoperiod of 16 h (light)/8 h (dark) (100 μmol m^{-2} s^{-1}) at 23 °C/20 °C. Siliques were opened using forceps and needles under a dissecting microscope (Leica MZ 16F). Images were acquired and processed using IM software and Adobe Photoshop (Adobe). To obtain nitrate-free mesophyll protoplasts, around

16–20 plants were grown on a Petri dish (150 mm × 15 mm) containing 100 ml of nitrogen-free 1 × MS medium salt, 0.1% MES, 1% sucrose, 0.7% phytoagar, 2.5 mM ammonium succinate and 0.5 mM glutamine, pH 6 under a photoperiod of 12 h (light)/12 h (dark) (75 μmol m^{-2} s^{-1}) at 23 °C/20 °C for 23–28 days. Mesophyll protoplasts were isolated from the second and the third pair of true leaves following the mesophyll protoplast isolation protocol[46]. To monitor plant growth without exogenous nitrogen source after germination, 30 seedlings were germinated and grown on a basal medium[11] (10 mM KH$_2$PO$_4$/KH$_2$PO$_4$, 1 mM MgSO$_4$, 1 mM CaCl$_2$, 0.1 mM FeSO$_4$-EDTA, 50 μM H$_3$BO$_3$, 12 μM MnSO$_4$·H$_2$O, 1 μM ZnCl$_2$, 1 μM CuSO$_4$·5H$_2$O, 0.2 μM Na$_2$MoO$_4$·2H$_2$O, 0.1% MES and 0.5% sucrose, pH 5.8) with 1% phytoagar under constant light (150 μmol m^{-2} s^{-1}) at 23 °C for 4 days. Photos were taken at different days (days 1–4) using a dissecting microscope (Leica MZ 16F) with IM software. To analyse the specific plant growth programs in response to different exogenous nitrogen sources at different concentrations, seedlings were germinated and grown on basal medium for 4 days as described above, and then transferred to the basal medium with 0.1, 0.5, 1, 5 or 10 mM KNO$_3$, NH$_4$Cl, glutamine or KCl for an additional 1–7 days. For gene expression analyses with RT–qPCR and RNA-seq, 10 seedlings were germinated in one well of the 6-well tissue culture plate (Falcon) with 1 ml of the basal medium supplemented with 2.5 mM ammonium succinate as the sole nitrogen source. Plates were sealed with parafilm and placed on the shaker at 70 r.p.m. under constant light (45 μmol m^{-2} s^{-1}) at 23 °C for 7 days. Before nitrate induction, seedlings were washed three times with 1 ml basal medium. Seedlings were treated in 1 ml of basal medium with KCl or KNO$_3$ for 15 min. Seedlings were then harvested for RNA extraction with TRIzol (Thermo Fisher Scientific). To block the kinase activity of CPK10(M141G), seedlings were pre-treated with 10 μM 3MBiP in the basal medium for 2 min, and then treated with KCl or KNO$_3$ for 15 min. For Ca^{2+} channel blockers and Ca^{2+} sensor inhibitors assays, seedlings were pre-treated with 2 mM LaCl$_3$, 2 mM GdCl$_3$, 250 μM W5 or 250 μM W7 in 1 ml of basal medium for 20 min, and then induced by 0.5 mM KCl or KNO$_3$ for 15 min. To monitor root morphology, seedlings were germinated and grown on a basal medium supplemented with 2.5 mM ammonium succinate and 1% phytoagar under constant light (150 μmol m^{-2} s^{-1}) at 23 °C for 3 days. Plants were then transferred to the basal medium supplemented with 1 μM 3MBiP and 5 mM KNO$_3$, 2.5 mM ammonium succinate, 5 mM KCl or 1 mM glutamine and grown for 5–8 days. After seedling transfer, 1 ml of 1 μM 3MBiP was added to the medium every 2 days. To monitor lateral root developmental stages, seedlings were monitored using a microscope (Leica DM5000B) with a 20× objective lens according to the protocol described previously[41]. To measure the primary and lateral root length, pictures were taken using a dissecting microscope (Leica MZ 16 F) with IM software and analysed by ImageJ. To compare the shoot phenotype, 8-day-old seedlings were cut above the root–shoot junction to measure the shoot fresh weight and acquire images. To analyse the *cpk* single-mutant phenotype, plants were germinated and grown on ammonium succinate medium for 3 days and then transferred to basal medium plates supplemented with 5 mM KNO$_3$ for 6 days. To analyse double mutants in response to 3MBiP, plants were transferred to basal medium plates supplemented with 5 mM KNO$_3$ and 1 μM 3MBiP for 6 days, and 3MBiP was reapplied every 2 days. Individual 9-day-old seedlings ($n = 12$) were collected to measure fresh weight and acquire images. To characterize the shoot phenotype of *nlp7-1* and the complementation lines, around 20 seeds were germinated on the Petri dish (150 mm × 15 mm) containing 100 ml of nitrogen-free 1 × MS medium salt (Caisson), 0.1% MES, 1% sucrose, 0.7% phytoagar and 25 mM KNO$_3$ medium pH 5.8 under a 16 h (light)/8 h (dark) photoperiod (100 μmol m^{-2} s^{-1}) at 18 °C and grown for 21 days. The shoots were collected for measurement of fresh weight and acquisition of images. For analyses of the shoot phenotype in icpk, seeds were germinated and grown on the ammonium succinate basal medium plate for 3 days and then transferred to the same medium supplemented with 1 μM 3MBiP. The inhibitor 3MBiP (5 ml of 1 μM) was reapplied on the medium twice during the growth.

Aequorin reconstitution and bioluminescence-based quantification of Ca^{2+} signals in whole seedlings. Two transgenic seedlings expressing apoaequorin[22] were germinated and grown in one well of a 12-well tissue culture plate (Falcon) with 0.5 ml of the basal medium supplemented with 2.5 mM ammonium succinate for 6 days. Individual plants were transferred to a luminometer cuvette filled with 100 μl of the reconstitution buffer (2 mM MES pH 5.7, 10 mM CaCl$_2$, and 10 μM native coelenterazine from NanoLight Technology) and incubated at room temperature in the dark overnight. The emission of photons was detected every second using the luminometer BD Monolight 3010. The measurement was initiated by injection of 100 μl 20 mM KCl, 20 mM KNO$_3$, 200 nM flg22 or ultrapure water into the cuvettes. Luminescence values were exported and processed using Microsoft Excel software.

GCaMP6-based Ca^{2+} imaging in mesophyll protoplasts and transgenic seedlings. For Ca^{2+} imaging in protoplasts, mesophyll protoplasts (2×10^5) in 1 ml buffer were co-transfected with 70 μg HBT-GCaMP6 and 50 μg

HBT-HY5-mCherry plasmid DNA. Transfected protoplasts were incubated in 5 ml of WI buffer[45] for 4 h. Before time-lapse recording, a coverslip was placed on a 10-well chamber slide covering three-quarters of a well, and placed on the microscope stage. Mesophyll protoplasts co-expressing GCaMP6 and HY5–mCherry (2×10^4 protoplast cells) were spun down for 1 min at 100g. WI-Ca^{2+} buffer (WI buffer plus 4 mM CaCl$_2$) (0.5 μl) with different stimuli (40 mM KCl, 40 mM KNO$_3$ or 40 mM NH$_4$Cl or 80 mM Ca^{2+} chelator (EGTA)) were added into 1.5 μl of concentrated mesophyll protoplasts in WI buffer. The final concentration of each stimulus was 10 mM KCl, 10 mM KNO$_3$, 10 mM NH$_4$Cl or 20 mM EGTA in the solution. The stimulated protoplasts were immediately loaded onto the slide and imaged via the Leica AF software on a Leica DM5000B microscope with the 20× objective lens. The exposure time for GCaMP6 was set at 1 s and recorded every 2 s to generate 199 frames. The exposure time was set at 45 ms for the bright field and 1 s for the mCherry signal. The fluorescence intensity was determined with the region of interest (ROI) function for each protoplast. The intensity data were exported and processed using Microsoft Excel software. The images were exported and processed using Adobe Photoshop software. To make a video, individual images were cropped using Adobe Photoshop software and saved in JPEG format. The videos were generated using ImageJ with the cropped images. For Ca^{2+} imaging with the *GCaMP6* transgenic seedling cotyledons, 5 seedlings were germinated in 1 well of a 6-well tissue culture plate (Falcon) with 1 ml of the basal medium supplemented with 2.5 mM ammonium succinate for 7 days. A chamber was made on microscope slides between two strips of the invisible tape (0.5 cm × 3 cm) and filled with 150 μl of the basal medium. A cotyledon of the 7-day-old seedling was cut in half using a razor blade and embedded in the medium. A thin layer of cotton was placed on top of the cotyledon to prevent moving. The coverslip was placed on the sample and fixed by another two strips of the invisible tape. The cotyledon was allowed to recover on the slide for 10 min. Confocal imaging was acquired using the Leica laser scanning confocal system (Leica TCS NT confocal microscope, SP1). The mesophyll cells in the cotyledon were targeted for Ca^{2+} imaging at the focal point. Basal medium (200 μl) with 10 mM KCl, 10 mM KNO$_3$ or 20 mM EGTA was loaded along one edge of the coverslip. A Kimwipes tissue on the opposite edge was used to draw the buffer into the chamber. To record fluorescence images, the excitation was provided at 488 nm and images were collected at emission 515–550 nm. The scanning resolution was set at 1,024 × 1,024 pixels. Images were captured every 10 s and averaged from two frames. In total, 80 images were collected and processed using Adobe Photoshop software. A video was generated with collected images using the method described above. For Ca^{2+} imaging with the *GCaMP6* transgenic seedling at the root tip and the elongated region of roots (around the middle region of the root), 10 seedlings were germinated and grown on the tissue culture plate (Falcon) with the basal medium and 1% phytoagar under constant light (150 μmol m^{-2} s^{-1}) at 23 °C for 4 days. The images were obtained using Leica laser scanning confocal system as described above for cotyledon Ca^{2+} imaging. In total, 33 images were collected and processed using Adobe Photoshop software. A video was generated with collected images using the method described above.

Mesophyll protoplast transient expression assays. Time-course, specificity and dosage analyses of *NIR-LUC* activity in response to nitrate induction was carried out in mesophyll protoplasts (2×10^4 protoplasts in 100 μl) co-transfected with 10 μg *NIR-LUC* and 2 μg *UBQ10-GUS* (as the internal control) and incubated in WI buffer[45] for 4 h, and then induced by 0.5 mM KCl, KNO$_3$, NH$_4^+$ or Gln or different concentrations of KNO$_3$ for 2 h. For time-course analysis, the fold change is calculated relative to the value of KCl treatment at each time point. For the nitrate-sensitized functional genomic screen, nitrate-free mesophyll protoplasts (2×10^4 protoplasts in 100 μl) were co-transfected with 8 μg HBT-CPKac (constitutively active CPK) or a control vector, 10 μg *NIR-LUC* and 2 μg *UBQ10-GUS* plasmid DNA, and incubated for 4 h to allow CPKac protein expression. To investigate the functional relationship between CPK10ac and NLP7 in nitrate signalling, nitrate-free mesophyll protoplasts (4×10^4 protoplasts in 200 μl) were co-transfected with 8 μg *NIR-LUC* and 2 μg *UBQ10-GUS* plasmid DNA, as well as 5 μg HBT-CPK10.0ac, HBT-CPK10ac(KM) or a control vector, or HBT-NLP7 or HBT-NLP7(S205A) in different combinations supplemented with 5 μg control vector to reach a total of 20 μg per transfection reaction, and incubated for 4 h for protein expression. Protoplasts were then induced with 0.5 mM KCl or KNO$_3$ for 2 h. The luciferase and GUS assay were carried out as described before[45]. The expression levels of NLP7-HA and CPK–Flag or CPK10ac–Flag in protoplasts were monitored by immunoblot with anti-HA-peroxidase (Roche, 11667475001; 1:2,000) and anti-Flag-HRP (Sigma, A8592; 1:2,000) antibodies, respectively.

Protein expression and purification. Expression vectors were transformed into Rosetta 2 (DE3) pLysS Competent Cells (Novagen). Cells were induced by 1 mM of IPTG when OD$_{600\,nm}$ reached 0.6, and proteins were expressed at 18 °C for 18 h. Affinity purification was carried out using HisTrap columns (GE Healthcare) and

the ÄKTA FPLC system. Purified proteins were buffer exchanged into PBS using PD-10 Desalting Columns (GE Healthcare), and then concentrated by Amicon Ultra-4 Centrifugal Filter Unit with Ultracel-10 membrane (EMD Millipore).

In-gel protein kinase assay. Around 10^6 protoplasts were incubated in WI buffer (5 ml) in Petri dishes (9 × 9 cm) for 4 h before induction with 10 mM KCl or KNO$_3$ for 10 min. Protoplasts were harvested and lysed in 200 μl of extraction buffer: 150 mM NaCl, 50 mM Tris-HCl pH 7.5, 5 mM EDTA, 1% Triton X-100, 1× protease inhibitor cocktail (Complete mini, Roche) and 1 mM DTT. The protein extract supernatant was obtained after centrifugation at 18,000g for 10 min at 4 °C. Total proteins (20 μg) were loaded on 8% SDS–PAGE embedded with or without 0.5 mg ml^{-1} histone type III-S (Sigma) as a general CPK phosphorylation substrate[23]. The gel was washed three times with washing buffer (25 mM Tris-HCl pH 7.5, 0.5 mM DTT, 5 mM NaF, 0.1 mM Na$_3$VO$_4$, 0.5 mg ml^{-1} BSA and 0.1% Triton X-100), and incubated for 20 h with three changes in the renaturation buffer (25 mM Tris-HCl pH 7.5, 0.5 mM DTT, 5 mM NaF and 0.1 mM Na$_3$VO$_4$) at 4 °C. The gel was then incubated in the reaction buffer (25 mM Tris-HCl pH 7.5, 2 mM EDTA, 12 mM MgCl$_2$, 1 mM CaCl$_2$, 1 mM MnCl$_2$, 1 mM DTT and 0.1 mM Na$_3$VO$_4$) with or without 20 mM EGTA at room temperature for 30 min. The kinase reaction was performed for 1 h in the reaction buffer supplemented with 25 μM cold ATP and 50 μCi [γ-^{32}P]ATP with or without 20 mM EGTA. The reaction was stopped by extensive washes in the washing buffer (5% trichloroacetic acid and 1% sodium pyrophosphate) for 6 h. The protein kinase activity was detected on the dried gel using the Typhoon imaging system (GE Healthcare).

3MBiP synthesis. 1-Isopropyl-3-(3-methylbenzyl)-1*H*-pyrazolo[3,4-*d*]pyrimidin-4-amine (3MBiP) was synthesized using the same procedures as those for a close structural analogue, 3MB-PP1 (ref. 39), with comparable yields, except that *iso*-propylhydrazine was substituted for *tert*-butylhydrazine.

^{1}H NMR (400 MHz, DMSO-d_6) δ 8.12 (s, 1H), 7.15 (d, J = 7.6 Hz, 1H), 7.08 (s, 1H), 7.00 (t, J = 7.5 Hz, 2H), 4.96 (p, J = 6.7 Hz, 1H), 4.31 (s, 2H), 2.24 (s, 3H), 1.44 (d, J = 6.7 Hz, 6H). ^{13}C NMR (100 MHz, DMSO-d_6) δ 158.41, 155.78, 153.69, 143.12, 139.56, 137.85, 129.51, 128.79, 127.30, 125.87, 98.92, 48.18, 40.10, 33.70, 22.23, 21.54. ESI–MS calculated for $C_{16}H_{20}N_5$ [M + H]$^+$ is 282.2, found 282.7.

***In vitro* protein kinase assays.** For *in vitro* kinase assay with CPK10(M141G)–Flag or CPK10–Flag, 4×10^4 protoplasts expressing CPK10(M141G)–Flag or CPK10–Flag were lysed in 200 μl immunoprecipitation buffer that contained 50 mM Tris-HCl pH 7.5, 150 mM NaCl, 5 mM EDTA, 1 mM DTT, 2 mM NaF, 2 mM Na$_3$VO$_4$, 1% Triton X-100 and 1× protease inhibitor cocktail (Complete mini, Roche). Protein extracts were incubated with 0.5 μg anti-Flag antibody (Sigma, F1804) at 4 °C for 2 h and an additional 1 h with protein G Sepharose beads (GE Healthcare). The immunoprecipitated kinase protein was washed three times with immunoprecipitation buffer and once with kinase buffer (20 mM Tris-HCl pH 7.5, 15 mM MgCl$_2$, 1 mM CaCl$_2$ and 1 mM DTT). Kinase reactions were performed for 1 h in 25 μl kinase buffer containing 1 μg histone (Sigma H5505 or H4524), 50 μM cold ATP and 2 μCi [γ-^{32}P]ATP. To block the CPK10(M141G)–Flag kinase activity, 1 μM 3MBiP or DMSO as a control was added in the 25 μl kinase buffer for 2 min before performing the kinase reaction. The reaction was stopped by adding SDS–PAGE loading buffer. After separation on a 12% SDS–PAGE gel, the protein kinase activity was detected on the dried gel using the Typhoon imaging system. For the *in vitro* kinase assay with CPK10(M141G)–HA isolated from *icpk10*,30 seedlings, 12 7-day-old seedlings grown in 2 wells of a 6-well-plate with 1 ml medium (0.5 × MS, 0.5% sucrose and 0.1% MES pH 5.7) were grounded in liquid nitrogen into powder and lysed in 200 μl of immunoprecipitation buffer. The CPK10(M141G)–HA protein was immunoprecipitated with the anti-HA antibody (Roche, 11666606001) and protein G Sepharose beads. *In vitro* kinase assay with CPK10(M141G)–HA proteins was carried out as described above. For the *in vitro* kinase assay with the subgroup III CPKs, Flag-tagged CPK7, CPK8, CPK10, CPK10(KM) (K92M, a kinase-dead mutation in the conserved ATP binding domain), CPK13, CPK30 and CPK32 were expressed in 10^5 protoplasts and purified with 1 μg anti-Flag antibody conjugated to protein G Sepharose beads as described above. CPK11–Flag from subgroup I was used as a negative control to demonstrate the specificity of NLP7 as a substrate for only subgroup III CPKs. NLP7–HIS (~1 μg) purified from *Escherichia coli* or histone type III-S (2 μg) was used as substrate in the *in vitro* kinase assay. Kinase reactions were performed for 1 h at 28 °C in 25 μl kinase buffer containing 5 μM cold ATP and 6 μCi [γ-^{32}P]ATP, which greatly enhanced the CPK activity. To reduce the background caused by free [γ-^{32}P]ATP in the gel, 50 μM cold ATP was added to the kinase reaction before sample loading in 10% (NLP7–HIS) or 12% (HIS) SDS–PAGE gel. To demonstrate that the kinase activities of CPK10, CPK30 and CPK32 were Ca^{2+}-dependent, 4×10^4 (CPK10 or CPK10ac) or 10^5 (CPK30, CPK32, CPK30ac or CPK32ac) protoplasts expressing CPKs for 12 h instead of 6 h (to increase the yield of CPK proteins) were lysed in 200 μl (CPK10) or 400 μl (CPK30 or CPK32) of immunoprecipitation buffer. The CPK proteins were immunoprecipitated with

anti-Flag antibody (0.5 μg for CPK10 or CPK10ac, and 2 μg for CPK30, CPK32, CPK30ac or CPK32ac) conjugated to protein G Sepharose beads. The immuno-precipitated CPKs were washed three times with immunoprecipitation buffer and twice with EGTA kinase buffer (20 mM Tris-HCl pH 7.5, 15 mM MgCl$_2$, 15 mM EGTA and 1 mM DTT). Kinase reactions were performed for 1 h at 28 °C in 25 μl kinase buffer or EGTA kinase buffer containing 5 μM cold ATP and 6 μCi [γ-^{32}P]ATP and purified NLP7–HIS (~1 μg), NLP7-N (1–581 amino acids) (~0.8 μg), NLP7-N(S205A) (~0.8 μg), or histone type III-S (2 μg). After performing the kinase reaction, 50 μM cold ATP was added to reduce the background caused by free [γ-^{32}P]ATP. The reaction was stopped by adding SDS–PAGE loading buffer. After separation on a 12% SDS–PAGE gel (histone type III-S) or 10% (NLP7–HIS or NLP7-N–HIS) SDS–PAGE gel, the protein kinase activity was detected on the dried gel using the Typhoon imaging system. Substrate was stained with InstantBlue Protein Stain (C.B.S. Scientific). The expression levels of CPK or CPKac proteins were monitored by immunoblot with anti-Flag-HRP (Sigma, A8592; 1:4,000) antibody. CPKac proteins without the Ca^{2+}-binding EF-hand domains provided constitutive kinase activities that were insensitive to EGTA. The sensitivity of CPK10, CPK30 and CPK32 to EGTA in kinase assays demonstrated their functions as Ca^{2+} sensors in nitrate signalling, which was further supported by the lack of NLP7–HA phosphorylation and the nuclear retention of NLP7–GFP in *icpk* mutant cells. Importantly, NLP7(S205A) lost nitrate-induced phosphorylation, nuclear localization, *NIR-LUC* activation, and endogenous target gene activation in wild-type protoplasts and seedlings.

RNA isolation, RT–PCR and RT–qPCR. RNA isolation, RT–PCR and RT–qPCR were carried out as described previously[11]. The primers used for RT–PCR and RT–qPCR are listed in Supplementary Table 5. *TUB4* was used as a control in wild-type and *cpk* mutants. The relative gene expression was normalized to the expression of *UBQ10*. Triplicate biological samples were analysed with consistent results.

RNA-seq analyses. We chose the early time point to minimize secondary target genes and the complexity that negative feedback would have introduced, including indirect effects from assimilation of nitrate and the subsequent activation of transcriptional repressors[1,3,4,8,10,13]. Seven-day-old wild-type and *icpk* seedlings were pretreated with 10 μM 3MBiP for 2 min and then treated for 15 min with either 10 mM KCl or 10 mM KNO$_3$. Total RNA (0.5 μg) was used for preparing the library with the Illumina TruSeq RNA sample Prep Kit v2 according to the manufacturer's guidelines with 9 different barcodes (triplicate biological samples). The libraries were sequenced for 50 cycles on an Illumina HiSeq 2500 rapid mode using two lanes of a flow cell. The sequencing was performed at MGH Next Generation Sequencing Core facility (Boston, USA). Fastq files, downloaded from the core facility, were used for data analysis. The quality of each sequencing library was assessed by examining fastq files with FastQC. Reads in the fastq file were first aligned to the *Arabidopsis* genome, TAIR10, using Tophat[51]. HTSeq[52] was used to determine the reads per gene. Finally, DESeq2 (ref. 53) analysis was performed to determine differential expression[54]. For HTSeq-normalized counts in each sample, differentially expressed genes were determined for wild-type KNO$_3$ versus wild-type KCl and *icpk* KNO$_3$ versus wild-type KNO$_3$. The differential expression analysis in DESeq2 uses a generalized linear model of the form

$$K_{ij} \sim NB(\mu_{ij}, a_i)$$

$$\mu_{ij} = s_j q_{ij}$$

$$\log_2(q_{ij}) = x_j \cdot \beta_i$$

where counts K_{ij} for gene i, sample j are modelled using a negative binomial (NB) distribution with fitted mean μ_{ij} and a gene-specific dispersion parameter α_i. The fitted mean is composed of a sample-specific size factor s_j and a parameter q_{ij} proportional to the expected true concentration of fragments for sample j. The coefficients β_i give the log$_2$ fold changes for gene i for each column of the model matrix *X*. Results were imported into Microsoft Excel for filtering. To generate a list to minimize false positives of primary nitrate-responsive genes in the wild type, we applied a relatively high stringency, $q \leq 0.05$ cut-off, followed by a log$_2 \leq -1$ or ≥ 1 cut-off.

To generate a heatmap, we performed agglomerative hierarchical clustering on genes with Gene Cluster 3.0 (ref. 55) using Correlation (uncentred) as the similarity metric and single linkage as the clustering method. Java Treeview[56] was used to visualize the results of the clustering. To obtain a list of enriched gene functions, we used the Classification SuperViewer Tool on the BAR website (http://bar.utoronto.ca/ntools/cgi-bin/ntools_classification_superviewer.cgi) with the MapMan classification source option. Analyses of enriched functional categories with nitrate upregulated and downregulated genes were performed using the MapMan classification source option on the Classification SuperViewer Tool with manual annotation based on literature. The fold enrichment is calculated as follows: (number in class$_{input\_set}$/

number of total$_{input\_set}$)/ (number in class$_{reference\_set}$/ number of total$_{reference\_set}$). The *P* value is calculated in Excel using a hypergeometric distribution test. The data in Extended Data Fig. 4c and d were sorted by fold enrichment with a $P < 0.05$ cut-off. For the biological duplicate RNA-seq experiments for identifying NLP7 target genes in the mesophyll protoplast transient expression system, 500 μg HBT-NLP7-HA, HBT-NLP7(S205A)-HA or control plasmid DNA was transfected into 10^6 protoplasts and incubated for 4.5 h. Total RNA (0.5 μg) was used to construct the libraries with six different barcodes (biological duplicate samples) as described above. The sequencing result was performed and analysed as described above. Differentially expressed genes were determined with DESeq2 on NLP7 versus Ctl (Control) and NLP7(S205A) versus Ctl. Results were imported into Microsoft Excel for filtering (log$_2 \geq 1$ cut-off) and generating heatmaps.

Immunoblot analyses of nitrate-induced phosphorylation of NLP6 and NLP7 *in vivo*. Transgenic seedlings expressing NLP6–MYC or NLP7–MYC were germinated and grown in basal medium containing 0.5 mM ammonium succinate as a sole nitrogen source (0.01% MES-KOH, pH 5.7) for 4 days at 23 °C under continuous light (60 μmol m^{-2} s^{-1}). After replacement with fresh medium supplemented with 10 mM KCl or KNO$_3$, the seedlings were collected after incubation for 5, 10 or 30 min. To examine the effects of Ca^{2+} channel blockers and Ca^{2+} sensor inhibitors, the 4-day-old seedlings were placed in fresh basal medium supplemented with 2 mM LaCl$_3$, 2 mM GdCl$_3$, 250 μM W5 or 250 μM W7 for 20 min and induced by 10 mM KCl or KNO$_3$. The seedlings were weighed, frozen in liquid nitrogen and ground using a Multibeads Shocker (Yasui Kikai). The ground samples were suspended in 20 volume of 1× Laemmli sample buffer supplemented with twice the concentration of EDTA-free protease inhibitor cocktail (Roche) and heated at 95 °C for 30 s. Samples were then spun down and the supernatant was subjected to SDS–PAGE and immunoblotting with anti-MYC (Millipore, 05-419; 1:1,000) and anti-histone H3 (Abcam, ab1791; 1:5,000) antibodies. For calf intestinal alkaline phosphatase (CIP) treatment, proteins in 1.2-fold CIP buffer (60 mM Tris-HCl pH 8.0, 120 mM NaCl, 12 mM MgCl$_2$, 1.2 mM DTT, 2.4-fold concentration of EDTA-free Protease Inhibitor Cocktail) were mixed with CIP solution (New England Biolabs, M0290, 10 U μl^{-1}) at a ratio of 5 (CIP buffer):1 (CIP solution) and incubated at 37 °C for 30 min. Heat-inactivated CIP was mixed as a control treatment. The reactions were stopped by adding an equal volume of 2× Laemmli sample buffer and heating at 95 °C for 30 s. To demonstrate that nitrate-induced NLP7 phosphorylation was abolished in *icpk* by protein mobility shift in SDS–PAGE, 4×10^4 protoplasts isolated from wild-type or *icpk* seedlings were transfected with 20 μg NLP7–HA or NLP7(S205A)–HA. To block CPK10(M141G) activity in *icpk*, 10 μM 3MBiP was added in the incubation buffer (WI) after transfection. After expressing protein for 4.5 h, protoplasts were induced by 10 mM KCl or KNO$_3$ for 15 min. Protoplasts were spun down and re-suspended in 40 μl 1× Laemmli sample buffer. Samples (10 μl) were separated in a 6% SDS–PAGE resolving gel without a stacking gel layer. After transferring proteins to the PVDF membrane, the NLP7 (wild-type and S205A) proteins were detected with anti-HA-peroxidase (Roche, 11667475001; 1:2,000). RuBisCo was detected by an anti-rubisco antibody (Sigma, GW23153; 1:5,000) as a loading control.

Detection of Ser205 phosphorylation in NLP7 *in vivo*. Transformation of T87 cell suspension culture derived from a seedling of *A. thaliana* L. (Heynh.) ecotype Columbia[57] was conducted with the 35SΩ-NLP7-MYC construct in the pCB302 binary plasmid carrying the hygromycin B selection marker gene. Transformants mediated by *Agrobacterium* (GV3101) were selected on agar plates (JPL medium, 3 g l^{-1} gellun gum, 500 mg l^{-1} carbenicillin and 20 mg l^{-1} hygromycin), and the transformants were maintained in liquid JPL medium as described previously[57]. T87 cells expressing NLP7–MYC were incubated in nitrogen-free JPL liquid medium for 2 days, and then 10 mM KNO$_3$ was added into the medium. After 30 min treatment, the T87 cells (approximately 4 g frozen weight) were frozen in liquid nitrogen and homogenized with Multi-beads Shocker (Yasui Kikai) in 10 ml of the buffer that contained 25 mM Tris-HCl pH 7.5, 150 mM NaCl, 0.1% NP-40, 10% glycerol, 1× Complete Protease Inhibitor Cocktail and 1× PhosSTOP (Roche). Cell lysates obtained were incubated with anti-MYC antibodies crosslinked to Dynabeads (Invitrogen). Trapped proteins were eluted by 1× Laemmli sample buffer and separated by SDS–PAGE. Gel pieces containing NLP7–MYC were recovered and subjected to in-gel double digestion with trypsin (10 ng μl^{-1}) and chymotrypsin (10 ng μl^{-1}) (Promega). NanoLC–ESI–MS/MS analysis was performed as described previously[58,59] with minor modifications.

NLP7, CPK10, CPK30 and CPK32 nuclear localization analyses. To analyse NLP7 nuclear retention triggered by nitrate in protoplasts, nitrate-free mesophyll protoplasts (4×10^4 protoplasts in 200 μl) were co-transfected with 20 μg NLP7–GFP or NLP7(S205A)–GFP and 10 μg HBT-HY5-mCherry plasmid DNA and incubated for 6 h. Mesophyll protoplasts were spun down for 1 min at 100*g*. WI buffer with 10 mM KCl or KNO$_3$ was added into mesophyll protoplasts for 30 min. The treated protoplasts were loaded onto slides and imaged with the 20× objective lens on a Leica DM5000B microscope operated with the Leica AF software.

The images were collected and processed using Adobe Photoshop software. To analyse NLP7–GFP nuclear retention triggered by nitrate in transgenic lines, NLP7–GFP/*nlp7-1* and NLP7(S205A)–GFP/*nlp7-1* seedlings were germinated and grown on the basal medium supplemented with 2.5 mM ammonium succinate and with 1% phytoagar under constant light (150 μmol m^{-2} s^{-1}) at 23 °C for 5 days. Plants were placed on the slide as described above and stimulated by 10 mM KNO$_3$. Confocal images were acquired as described for GCaMP6-based Ca^{2+} imaging in transgenic seedlings. To analyse CPK10, CPK30 and CPK32 nuclear localization in response to nitrate, nitrate-free mesophyll protoplasts (4×10^4 protoplasts in 200 μl) were co-transfected with 20 μg CPK10–GFP, CPK30–GFP or CPK32–GFP and 10 μg HBT-HY5-mCherry plasmid DNA and incubated for 12 h. Protoplasts were then treated with 10 mM KNO$_3$ for 5 min. Confocal imaging was acquired using the Leica Application Suite X software on a Leica TCS SP8 (Leica) confocal microscope with the 40× objective lens. To obtain fluorescence images, the excitation was set to 489 nm (GFP) and 587 nm (mCherry), and images at emissions 508 nm (GFP) and 610 nm (mCherry) were collected. The scanning resolution was set to 1,024 × 1,024 pixels. The images were collected and processed using Adobe Photoshop software. To analyse NLP7–GFP nuclear retention in wild-type and *icpk* seedlings, nitrate-free mesophyll protoplasts (4×10^4 protoplasts in 200 μl) were co-transfected with 20 μg NLP7–GFP and 4 μg HBT-Td-Tomato plasmid DNA and incubated for 12–16 h. The transfected protoplasts were treated with inhibitor 10 μM 3MBiP 30 min before nitrate induction. Protoplasts were treated with 10 mM KNO$_3$ for 15 min in the presence of 10 μM 3MBiP of WI buffer. The images were acquired as described above for the NLP7 nuclear retention in protoplasts.

BiFC assay. Nitrate-free mesophyll protoplasts (4×10^4 protoplasts in 200 μl) were co-transfected with 18 μg UBQ10-CPK10(KM)-YN, UBQ10-NLP7-YC, and 4 μg HBT-HY5-mCherry plasmid DNA, and incubated for 12–18 h. Protoplasts were then treated with 10 mM KNO$_3$ for 2 h. Confocal images were acquired as described above for CPK localization in response to nitrate.
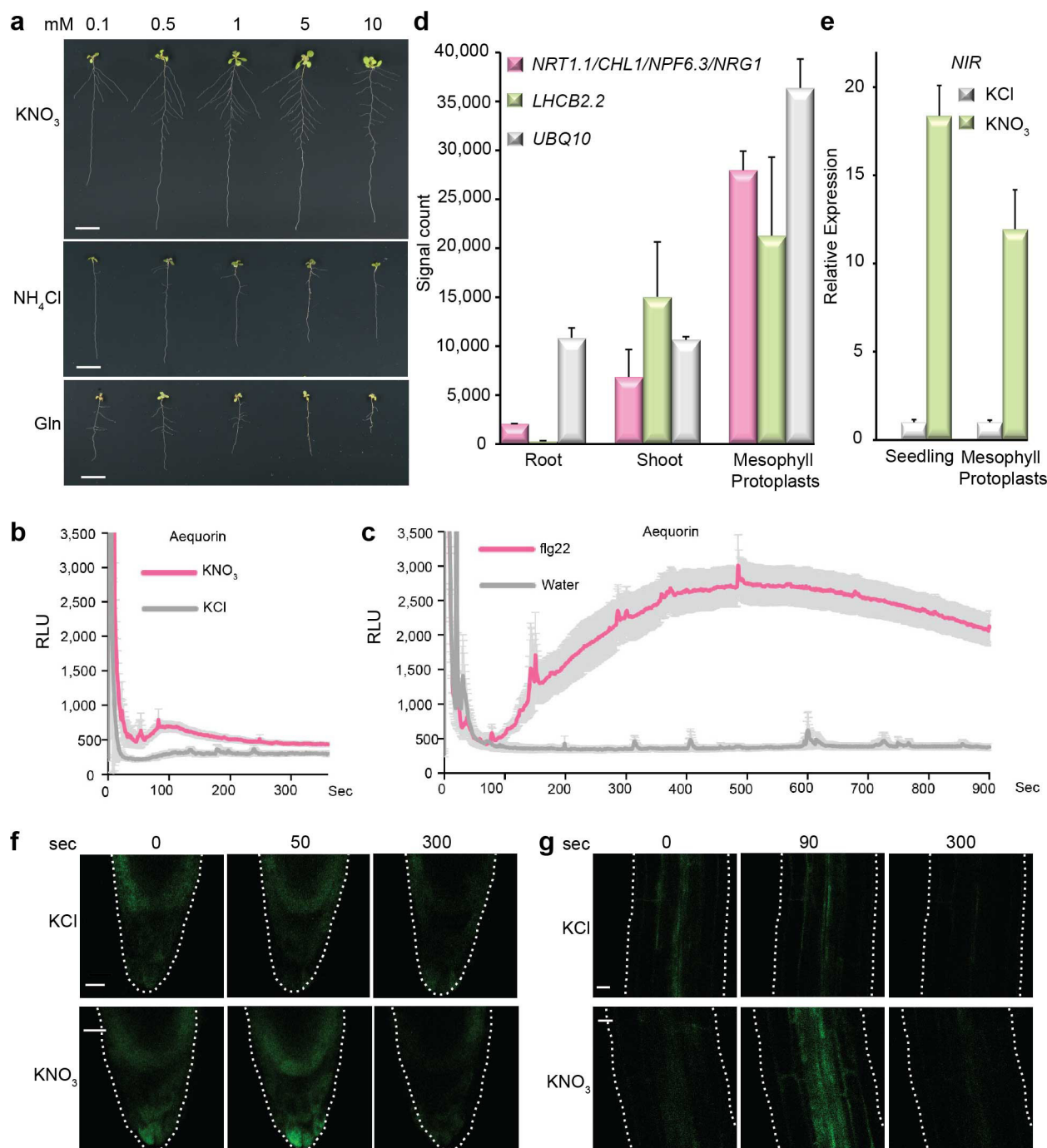
Statistical analysis. The chosen sample sizes for all experiments were empirically determined by measuring the mean and s.d. for the sample population in pilot experiments, and then calculated (the 1-sample Z-test method, two-sided test) with the aim to obtain the expected mean of less than 25% significant difference with the alpha value ≤ 0.05 and the power of the test ≥ 0.80. For multiple comparisons, data were first subjected to one-way or two-way ANOVA, followed by Tukey's multiple comparisons test to determine statistical significance. To compare two groups, a Student's *t*-test was used instead. To compare wild-type and *icpk* lateral root development, data were categorized into two groups, and then subjected to a chi-square test, as indicated in the figure legends. Experiments were not randomized and investigators were not blinded to allocation during experiments and outcome assessment.

Data availability. RNA-seq data are available at the Gene Expression Omnibus (GEO) under accession number GSE73437. The Source Data for blots, gels and histograms are provided in the Supplementary Information. All other data are available from the corresponding author upon reasonable request.

45. Yoo, S. D., Cho, Y. H. & Sheen, J. *Arabidopsis* mesophyll protoplasts: a versatile cell system for transient gene expression analysis. *Nat. Protocols* **2**, 1565–1572 (2007).
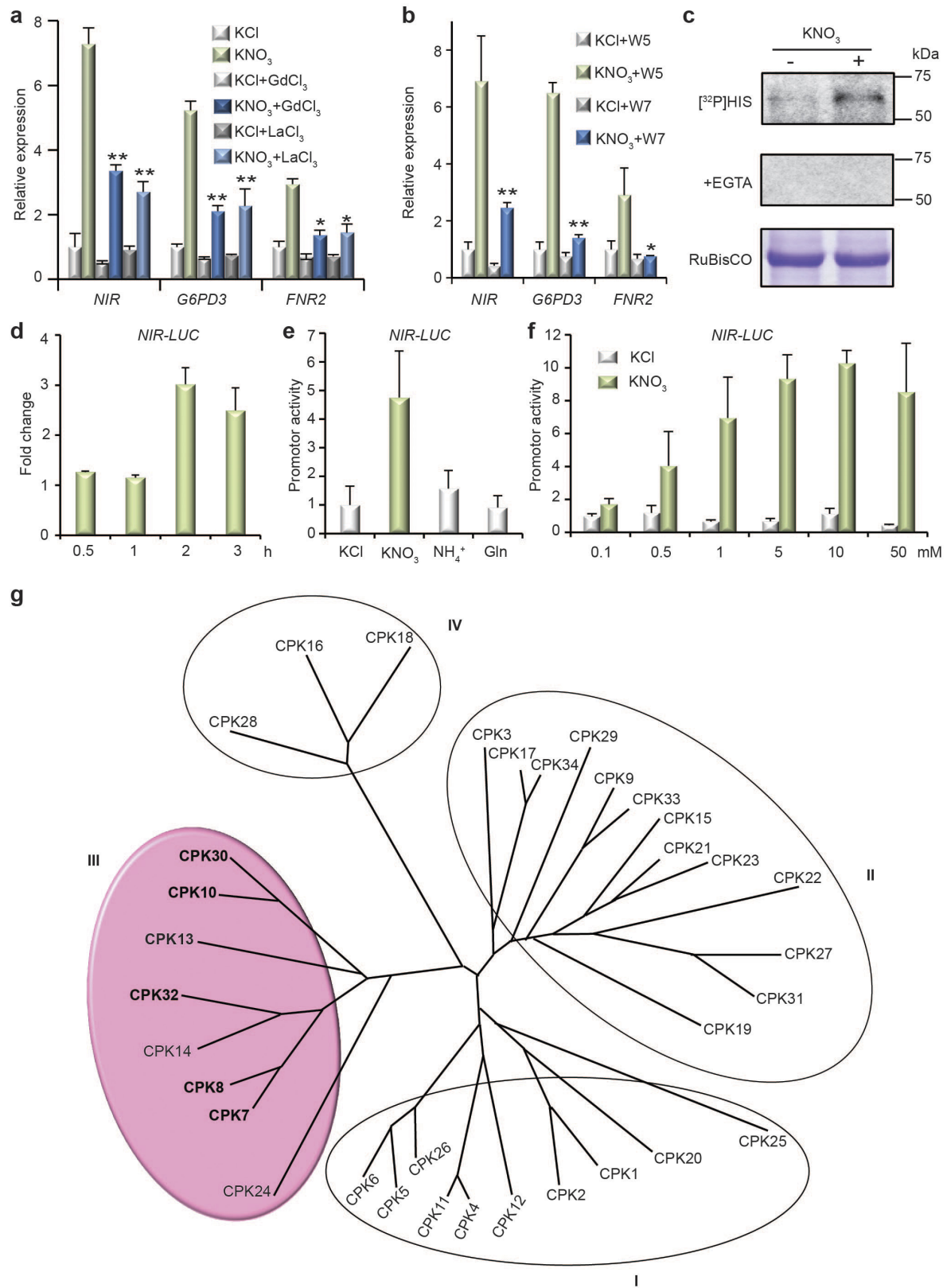
46. Xiang, C., Han, P., Lutziger, I., Wang, K. & Oliver, D. J. A mini binary vector series for plant transformation. *Plant Mol. Biol.* **40**, 711–717 (1999).
47. Clough, S. J. & Bent, A. F. Floral dip: a simplified method for *Agrobacterium*-mediated transformation of *Arabidopsis thaliana*. *Plant J.* **16**, 735–743 (1998).
48. Guo, J. *et al.* Involvement of *Arabidopsis* RACK1 in protein translation and its regulation by abscisic acid. *Plant Physiol.* **155**, 370–383 (2011).
49. Kato, Y., Konishi, M., Shigyo, M., Yoneyama, T. & Yanagisawa, S. Characterization of plant eukaryotic translation initiation factor 6 (eIF6) genes: The essential role in embryogenesis and their differential expression in *Arabidopsis* and rice. *Biochem. Biophys. Res. Commun.* **397**, 673–678 (2010).
50. Alonso, J. M. *et al.* Genome-wide insertional mutagenesis of *Arabidopsis thaliana*. *Science* **301**, 653–657 (2003).
51. Kim, D. *et al.* TopHat2: accurate alignment of transcriptomes in the presence of insertions, deletions and gene fusions. *Genome Biol.* **14**, R36 (2013).
52. Anders, S., Pyl, P. T. & Huber, W. HTSeq—a Python framework to work with high-throughput sequencing data. *Bioinformatics* **31**, 166–169 (2015).
53. Love, M. I., Huber, W. & Anders, S. Moderated estimation of fold change and dispersion for RNA-seq data with DESeq2. *Genome Biol.* **15**, 550 (2014).
54. Van Verk, M. C., Hickman, R., Pieterse, C. M. & Van Wees, S. C. RNA-Seq: revelation of the messengers. *Trends Plant Sci.* **18**, 175–179 (2013).
55. de Hoon, M. J., Imoto, S., Nolan, J. & Miyano, S. Open source clustering software. *Bioinformatics* **20**, 1453–1454 (2004).
56. Saldanha, A. J. Java Treeview–extensible visualization of microarray data. *Bioinformatics* **20**, 3246–3248 (2004).
57. Axelos, M., Curic, C., Mazzolini, L., Bardet, C. & Lescure, N. A protocol for transient gene expression in *Arabidopsis thaliana* protoplasts isolated from cell suspension cultures. *Plant Physiol. Biochem.* **30**, 123–128 (1992).
58. Aki, T., Shigyo, M., Nakano, R., Yoneyama, T. & Yanagisawa, S. Nano scale proteomics revealed the presence of regulatory proteins including three FT-Like proteins in phloem and xylem saps from rice. *Plant Cell Physiol.* **49**, 767–790 (2008).
59. Aki, T. & Yanagisawa, S. Application of rice nuclear proteome analysis to the identification of evolutionarily conserved and glucose-responsive nuclear proteins. *J. Proteome Res.* **8**, 3912–3924 (2009).
60. Baena-González, E., Rolland, F., Thevelein, J. M. & Sheen, J. A central integrator of transcription networks in plant stress and energy signalling. *Nature* **448**, 938–942 (2007).
61. Cheng, S. H., Willmann, M. R., Chen, H. C. & Sheen, J. Calcium signaling through protein kinases. The *Arabidopsis* calcium-dependent protein kinase gene family. *Plant Physiol.* **129**, 469–485 (2002).
62. Curran, A. *et al.* Calcium-dependent protein kinases from *Arabidopsis* show substrate specificity differences in an analysis of 103 substrates. *Front. Plant Sci.* **2**, 36 (2011).
63. Song, C. *et al.* Systematic analysis of protein phosphorylation networks from phosphoproteomic data. *Mol. Cell. Proteomics* **11**, 1070–1083 (2012).
64. Yaffe, M. B. *et al.* A motif-based profile scanning approach for genome-wide prediction of signaling pathways. *Nat. Biotechnol.* **19**, 348–353 (2001).
65. Soyano, T., Shimoda, Y. & Hayashi, M. NODULE INCEPTION antagonistically regulates gene expression with nitrate in *Lotus japonicus*. *Plant Cell Physiol.* **56**, 368–376 (2015).
66. Suzuki, W., Konishi, M. & Yanagisawa, S. The evolutionary events necessary for the emergence of symbiotic nitrogen fixation in legumes may involve a loss of nitrate responsiveness of the NIN transcription factor. *Plant Signal. Behav.* **8**, e25975 (2013).
67. O'Malley, R. C. *et al.* Cistrome and epicistrome features shape the regulatory DNA landscape. *Cell* **165**, 1280–1292 (2016).

Extended Data Figure 1 | Nitrate promotes plant development and induces Ca²⁺ signatures in leaves and roots. a, Nitrate promotes shoot and root development. Plants were germinated without an exogenous nitrogen source for 4 days and then transferred to the plates supplemented with different concentrations of KNO₃, NH₄Cl or glutamine for 7 days. Scale bars, 1 cm. The experiments were repeated twice with 10 seedlings for each treatment with consistent results. **b, c**, Distinct Ca²⁺ signatures induced by nitrate and flg22 in aequorin transgenic plants. *Arabidopsis* transgenic seedlings constitutively expressing the Ca²⁺ reporter protein apoaequorin were grown in liquid medium containing 2.5 mM ammonium succinate as the sole nitrogen source for 6 days. Aequorin was reconstituted with 10 μM coelenterazine overnight in the dark. The results are presented as relative light units (RLU) in response to 10 mM KCl or KNO₃ (**b**) or to 100 nM flg22 or water (**c**) at intervals of 1 s. Error bars, ± s.e.m., *n* = 10 seedlings. The experiments were repeated three times with similar results. The RLU value is cut-off at 3,500. **d**, *NRT1.1* is highly expressed in shoots and mesophyll protoplasts. The signal counts of the genes in roots and shoots were derived from previously published

microarray data[4]. The signal counts of the genes for mesophyll protoplasts were derived from previously published microarray data[60]. *LHCB2.2* serves as a leaf-specific expression control. The control gene *UBQ10* is constitutively and highly expressed in roots, shoots and mesophyll protoplasts. Error bars, s.d., *n* = 3 biological replicates from mesophyll protoplasts. **e**, Nitrate induction of the endogenous *NIR* gene as a primary nitrate-responsive marker gene in seedlings and mesophyll protoplasts. *NIR* expression was quantified by RT–qPCR analysis. *Arabidopsis* seedlings or mesophyll protoplasts were treated with 10 mM KCl or KNO₃ for 2 h. Error bars, s.d., *n* = 3 biological replicates. **f, g**, Time-lapse images of nitrate-stimulated Ca²⁺ signalling in roots of intact transgenic GCaMP6 plants. The entire time-lapse recording of Ca²⁺ signals stimulated by 10 mM KCl or KNO₃ in the root tip (**f**) or the elongated region (**g**) is shown in Supplementary Videos 3 and 4. Seedlings were grown on basal medium without nitrogen for 4 days and then stimulated by KCl or KNO₃. Scale bars, 10 μm. The experiments were repeated three times with 10 seedlings for each treatment with consistent results. Source Data for **d** and **e** can be found in the Supplementary Information.
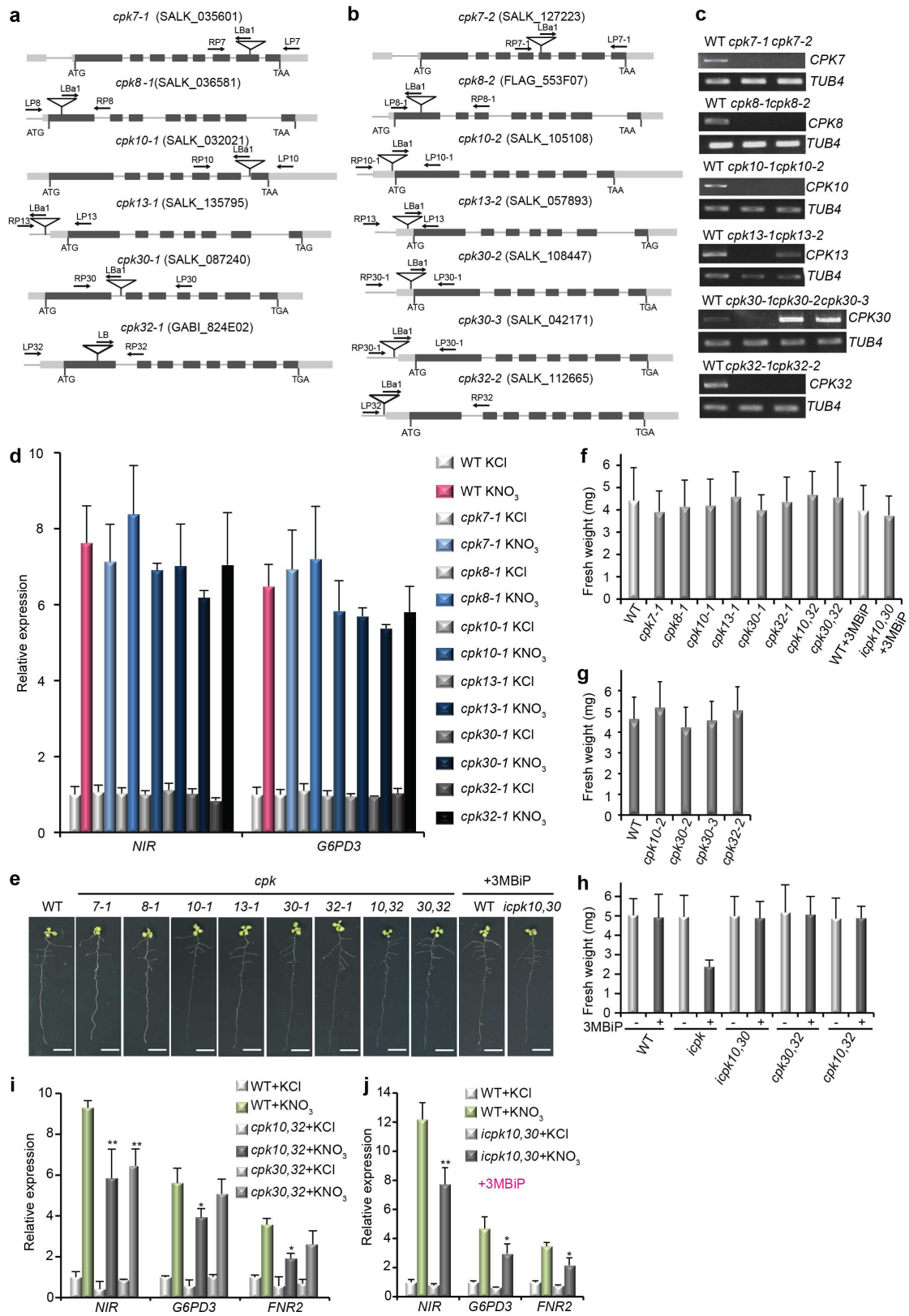
Extended Data Figure 2 | See next page for caption.

Extended Data Figure 2 | Calcium mediates the nitrate response in seedlings and mesophyll protoplasts. a, Ca^{2+} channel blockers diminish primary nitrate-responsive transcription. RT–qPCR analyses with 7-day-old seedlings. 0.5 mM KNO_3, 15 min. Error bars, s.d., $n = 3$ biological replicates. $*P < 0.05$, $**P < 0.0001$ (two-way ANOVA with Tukey's multiple comparisons test). **b**, An antagonist of Ca^{2+} sensors (W7) inhibits primary nitrate-responsive transcription. Error bars, s.d., $n = 3$ biological replicates. $*P < 0.05$, $**P < 0.0001$ (two-way ANOVA with Tukey's multiple comparisons test). **c**, Nitrate stimulates putative endogenous CPKs in an in-gel kinase assay. 10 mM KNO_3, 10 min. **d**, Time-course analysis of *NIR-LUC* activity in response to nitrate induction. Mesophyll protoplasts co-transfected with *NIR-LUC* and *UBQ10-GUS* (as the internal control) were incubated in WI buffer for 4 h and then induced by 0.5 mM KCl or KNO_3 for 0.5, 1, 2 and 3 h. The fold change is calculated relative to the value of KCl treatment at each time point. Error bars, s.d., $n = 3$ biological replicates. **e**, Nitrate-specific induction of *NIR-LUC* expression. Transfected mesophyll protoplasts were incubated in WI buffer for 4 h and then induced by 0.5 mM KCl or different nitrogen sources for 2 h. Error bars, s.d., $n = 3$ biological replicates. **f**, Sensitive regulation of *NIR-LUC* by nitrate. Transfected mesophyll protoplasts were incubated in WI buffer for 4 h and then induced by different concentration of KCl or KNO_3 for 2 h. Error bars, s.d., $n = 3$ biological replicates. **g**, Relation tree of *Arabidopsis* CPK proteins. The relation tree was generated by ClustalX and Treeview algorithms using the complete protein sequences of CPKs. The subgroup III CPKs that enhanced *NIR-LUC* activity by more than two-fold are highlighted. Genes encoding CPK14 and CPK24 are not expressed in mesophyll cells. Source Data for **a**, **b**, **d**–**f** can be found in the Supplementary Information.
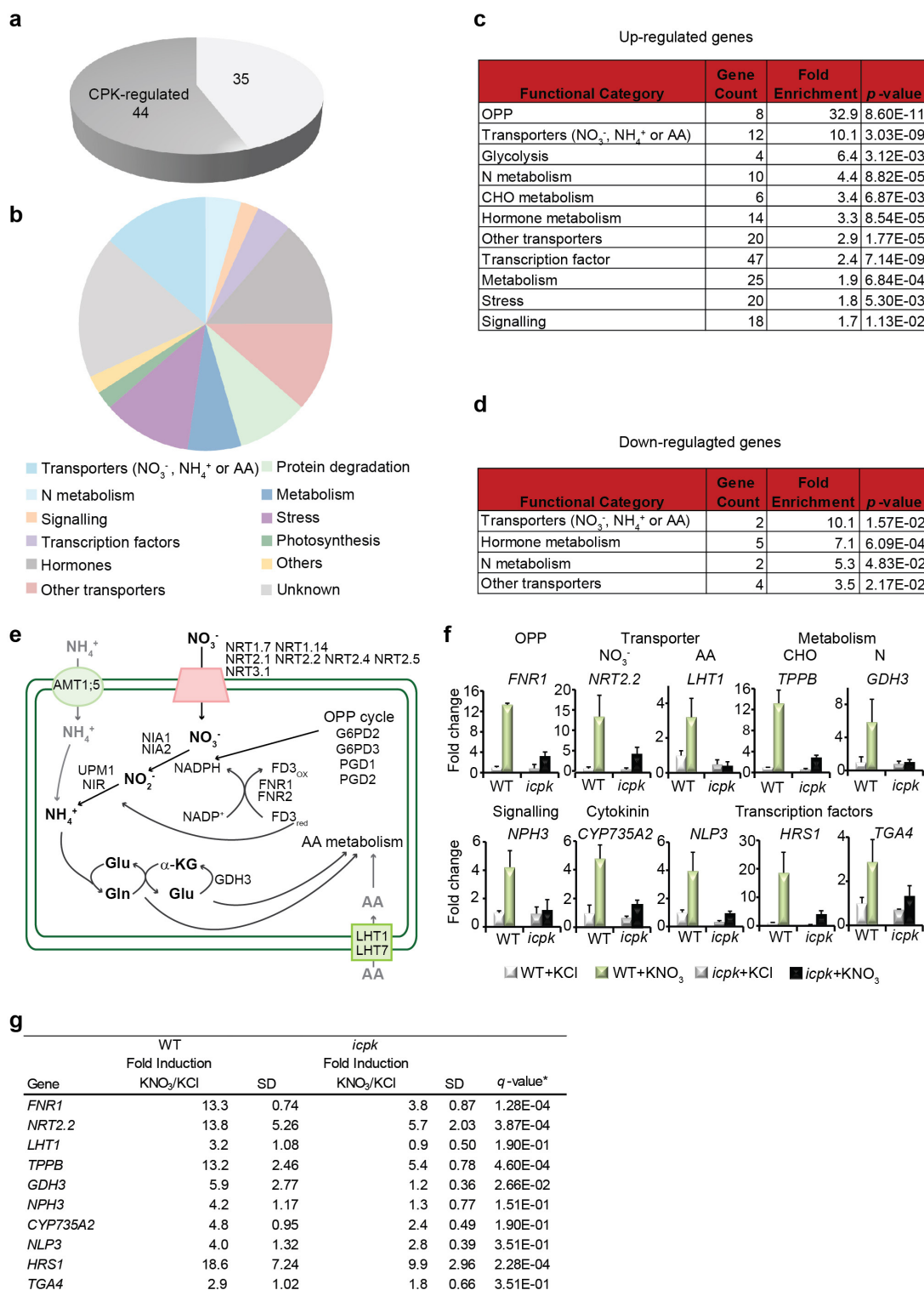
Extended Data Figure 3 | See next page for caption.

Extended Data Figure 3 | Analyses of single and double *cpk* and *icpk* mutants in subgroup III CPKs. a, **b**, The *cpk* T-DNA insertion lines. All *cpk* mutants were isolated and confirmed by PCR analysis of genomic DNA using gene-specific primers and a T-DNA left-border primer. Lines represent introns or promoters, whereas dark and light grey boxes represent exons and untranslated regions, respectively. Arrows represent primers used for genotyping (see Supplementary Table 4). **c**, RT–PCR analysis of *CPK* transcripts in *cpk* mutants. *TUB4* is the housekeeping control gene. **d**, Analyses of nitrate-responsive marker gene expression in *cpk* mutants. Seedlings (7-day-old) were induced by 0.5 mM KCl or KNO$_3$ for 15 min. Relative expression of nitrate-responsive marker genes was analysed by RT–qPCR and normalized to the expression of *UBQ10*. The expression level is calculated relative to the value of wild-type seedlings treated with KCl. Error bars, s.d., $n = 3$ biological replicates. **e**, Single and double *cpk* mutants lack an overt phenotype. Plants were germinated and grown on the ammonium succinate medium for 3 days and then transferred to basal medium plates supplemented with 5 mM KNO$_3$ for 6 days. To analyse the chemical analogue-sensitive mutants, wild-type and *icpk10,30* seedlings were transferred to basal medium plates supplemented with 5 mM KNO$_3$ and 1 μM 3MBiP for 6 days, and 3MBiP was reapplied every 2 days after transfer. Scale bar, 1 cm. Images are representative of 10 seedlings. **f**, **g**, The average fresh weight of 9-day-old single and double *cpk* mutants. Error bars, s.d., $n = 12$ seedlings. **h**, The average fresh weight of 9-day-old double *cpk* mutants and *icpk* supplemented with or without 3MBiP. Error bars, s.d., $n = 12$ seedlings. **i**, **j**, Primary nitrate-responsive gene expression is reduced in *cpk* double mutants. RT–qPCR analyses with 7-day-old seedlings. 0.5 mM KNO$_3$, 15 min. Error bars, s.d., $n = 3$ seedlings. *$P < 0.05$, **$P < 0.0001$ (two-way ANOVA with Tukey's multiple comparisons test). Source Data for **d**, **i** and **j** can be found in the Supplementary Information.

a

CPK-regulated 44 | 35

b

Transporters (NO_3^-, NH_4^+ or AA) | Protein degradation
N metabolism | Metabolism
Signalling | Stress
Transcription factors | Photosynthesis
Hormones | Others
Other transporters | Unknown

c

Up-regulated genes

Functional Category	Gene Count	Fold Enrichment	p-value
OPP	8	32.9	8.60E-11
Transporters (NO_3^-, NH_4^+ or AA)	12	10.1	3.03E-09
Glycolysis	4	6.4	3.12E-03
N metabolism	10	4.4	8.82E-05
CHO metabolism	6	3.4	6.87E-03
Hormone metabolism	14	3.3	8.54E-05
Other transporters	20	2.9	1.77E-05
Transcription factor	47	2.4	7.14E-09
Metabolism	25	1.9	6.84E-04
Stress	20	1.8	5.30E-03
Signalling	18	1.7	1.13E-02

d

Down-regulagted genes

Functional Category	Gene Count	Fold Enrichment	p-value
Transporters (NO_3^-, NH_4^+ or AA)	2	10.1	1.57E-02
Hormone metabolism	5	7.1	6.09E-04
N metabolism	2	5.3	4.83E-02
Other transporters	4	3.5	2.17E-02

e

f

WT+KCl | WT+KNO$_3$ | icpk+KCl | icpk+KNO$_3$

g

Gene	WT Fold Induction KNO$_3$/KCl	SD	icpk Fold Induction KNO$_3$/KCl	SD	q-value*
FNR1	13.3	0.74	3.8	0.87	1.28E-04
NRT2.2	13.8	5.26	5.7	2.03	3.87E-04
LHT1	3.2	1.08	0.9	0.50	1.90E-01
TPPB	13.2	2.46	5.4	0.78	4.60E-04
GDH3	5.9	2.77	1.2	0.36	2.66E-02
NPH3	4.2	1.17	1.3	0.77	1.51E-01
CYP735A2	4.8	0.95	2.4	0.49	1.90E-01
NLP3	4.0	1.32	2.8	0.39	3.51E-01
HRS1	18.6	7.24	9.9	2.96	2.28E-04
TGA4	2.9	1.02	1.8	0.66	3.51E-01

*:FDR (False Discovery Rate). Two-stage step-up method of Benjamini, Krieger and Yekutieli

Extended Data Figure 4 | RNA-seq and qRT–PCR data analyses and functional classification. Biological triplicate RNA-seq experiments were performed and analysed with DESeq2. **a**, Nitrate–CPK-downregulated genes. Dark grey, nitrate–CPK target genes ($q \leq 0.05$). **b**, Classification of nitrate–CPK-downregulated genes. The MapMan functional categories for nitrate-downregulated genes are presented. **c**, Enriched functional categories of nitrate-upregulated genes. **d**, Enriched functional categories of nitrate-downregulated genes. The fold enrichment is calculated as follows: (number of classified_input_set/number of total_input_set)/ (number of classified_reference_set/number of total_reference_set). The P value is calculated in Excel using a hypergeometric distribution test.
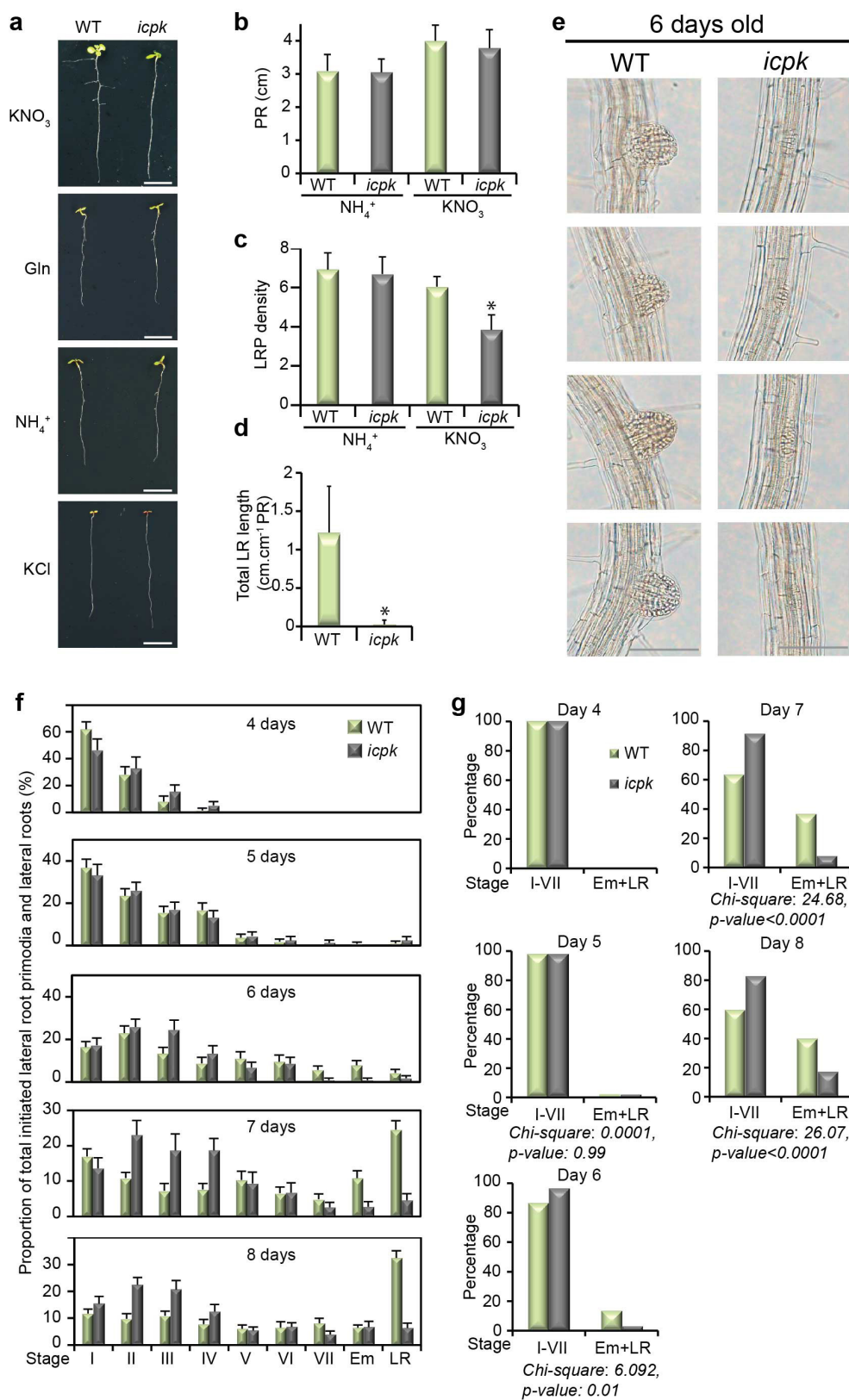
The categories were sorted by fold enrichment with a $P \leq 0.05$ cut-off. **e**, Nitrate–CPK target genes regulate nitrogen transport and metabolism. **f**, RT–qPCR analyses of nitrate–CPK target genes in eight functional classes in seedlings. 10 mM KNO$_3$, 15 min. Error bars, s.d., $n = 3$ biological replicates. *NIA1/2*, *NIR*, *NRT2.1/2.2*, *G6PD2/3*, *GLN*, *GDH3*, *UPM1*, *FD3* and *FNR1/2* genes were regulated by the CPK10, CPK30 and CPK32 protein kinases[1,3–5,12,13,16,28]. Transcription factor genes *NLP3*, *HRS1* and *TGA4* were primary nitrate–CPK target genes[3,12,13,15,20]. **g**, The fold changes of expression levels of nitrate-upregulated genes in wild-type and *icpk* seedlings listed in **f**. The table provided the Source Data for the histograms presented in **f**. $n = 3$ biological replicates.

Extended Data Figure 5 | Primary nitrate-upregulated genes are present in diverse experimental systems. Venn diagrams (http://www.cmbi.ru.nl/cdd/biovenn/) were used to present the comparison and overlaps between the list of primary nitrate-upregulated genes defined in this study and the nitrate-upregulated genes at 20 min defined by previously published gene sets[4,10,13]. Red, 394 nitrate-upregulated genes identified in this study with a $\log_2 \geq 1$ and $q \leq 0.05$ cut-off; light red, 992 nitrate-upregulated genes in this study with a $q \leq 0.05$ cut-off; dark blue, 338 nitrate-upregulated genes from ref. 4 with a $\log_2 \geq 1$ cut-off for both biological duplicate datasets; green, 366 nitrate-upregulated genes from the ref. 10 dataset with a $\log_2 \geq 1$ cut-off; light blue, 227 nitrate-upregulated genes from ref. 13 with a $\log_2 \geq 1$ cut-off. Gene numbers in each group and the percentage of overlapped nitrate-upregulated genes in previously published datasets are shown.
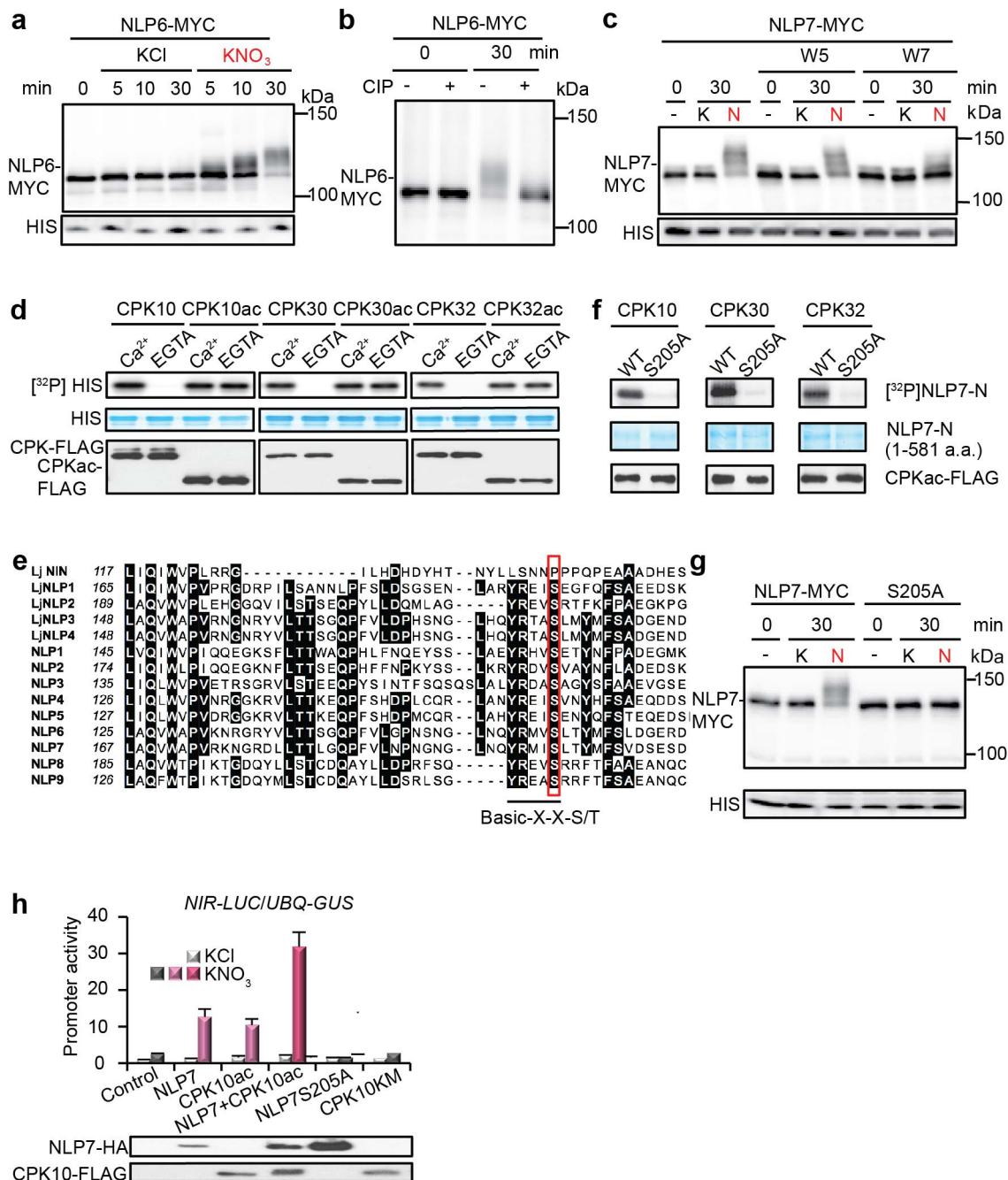
Extended Data Figure 6 | See next page for caption.

Extended Data Figure 6 | Quantitative analyses of root growth phenotype in wild-type and *icpk* seedlings in response to ammonium and nitrate. a, The *icpk* mutant displays defects in nitrate-stimulated lateral root establishment. Wild-type and *icpk* mutant seedlings were germinated and grown on ammonium succinate medium for 3 days, and then transferred to a plate supplemented with 5 mM KNO$_3$, 2.5 mM ammonium succinate, 5 mM KCl or 5 mM glutamine in the presence of 1 μM 3MBiP for 5 days. Scale bars, 1 cm. Images are representative of 6 seedlings. **b**, Primary root (PR) length was similar in 8-day-old wild-type and *icpk* seedlings. Error bars, s.d., $n = 16$ seedlings. **c**, Lateral root primordium (LRP) density decreased significantly in 8-day-old *icpk* seedlings in response to nitrate. Error bars, s.d., $n = 15$ seedlings. *$P < 0.05$ (Student's *t*-test). **d**, Lateral root (LR) length was markedly reduced in *icpk* seedlings in the presence of nitrate. Error bars, s.d., $n = 10$ seedlings. *$P < 0.05$ (Student's *t*-test). **e**, The development of lateral roots is severely retarded in *icpk*. The developmental stages of the third lateral root in 6-day-old wild-type and *icpk* seedlings induced by nitrate for 3 days are shown. Scale bars, 100 μm. Images are representative of 6 seedlings. **f**, Time-course analyses of *icpk* defects in nitrate-specific lateral root development stages I–VII[41]. Em, emerged primordia. Error bars, s.e.m., $n = 16$ seedlings. **g**, Chi-square test of wild-type and *icpk* lateral root development. Wild-type and *icpk* seedlings were compared on two categories, early lateral root development stages before emergence (stage I–VII) and afterwards (Em + LR). The low *P* value indicates the high level of association between the genotype and development stages.
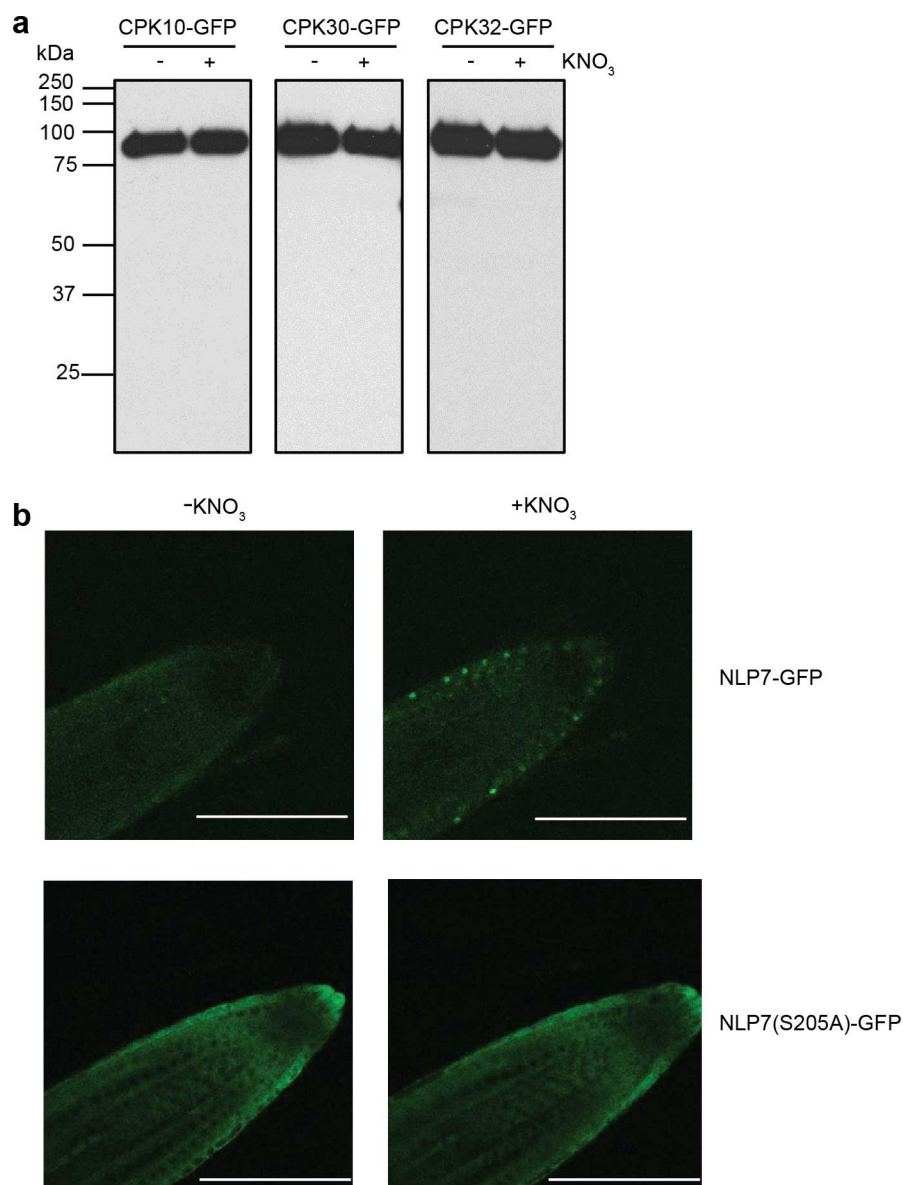
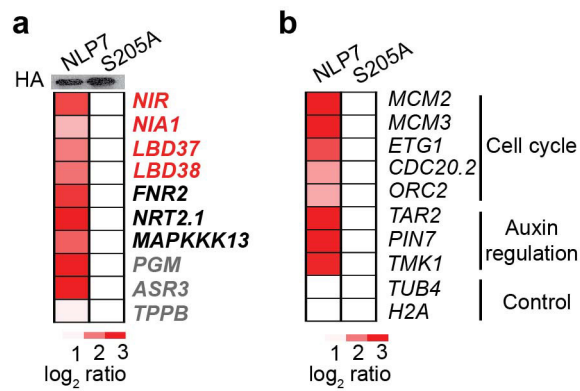**Extended Data Figure 7 | Nitrate-induced NLP phosphorylation.**
a, Nitrate-induced mobility shift of MYC-tagged NLP6. Transgenic seedlings expressing MYC-tagged NLP6 were grown in liquid medium containing 0.5 mM ammonium succinate as a sole nitrogen source for 4 days and then treated with 10 mM KCl or KNO_3 for indicated periods. Immunoblot analysis was carried out with proteins extracted from the seedlings using anti-MYC and anti-histone H3 (HIS) antibodies. **b**, Effect of alkaline phosphatase treatment on mobility shift of MYC-tagged NLP6. Proteins from seedlings treated with 10 mM KNO_3 for 0 or 30 min were subjected to CIP treatment. The experiments were repeated twice with consistent results. **c**, An antagonist of Ca^{2+} sensors (W7) diminished nitrate-triggered phosphorylation of NLP7. **d**, Phosphorylation of histone by CPK10, CPK30 and CPK32 is Ca^{2+}-dependent. **e**, Alignment of the amino acid sequences around the conserved CPK phosphorylation site in all NLPs from *A. thaliana* and *L. japonicus* (Lj). Conserved amino acid residues are indicated by black boxes. The CPK phosphorylation motif indicated by an underline was identified by multiple web-based

bioinformatics tools and literature analysis[61–66] with a candidate serine (Ser205 in NLP7) that is uniquely conserved in nine *Arabidopsis* NLPs and four orthologous *L. japonicus* NLPs (outlined in red), but not in *L. japonicus* NIN. *Lj*NIN, a variant of NLP, which evolved specifically for symbiotic nitrogen fixation in legumes, lacks a CPK phosphorylation site. **f**, Ser205 in NLP7 is the phosphorylation site for CPK10, CPK30 and CPK32. **g**, Nitrate-induced mobility shift was abolished for NLP7(S205A). **h**, Overexpression of NLP7 and CPK10ac showed similar synergism with nitrate for *NIR-LUC* activation in protoplast transient assays. NLP7 or CPK10ac alone was not effective to enhance *NIR-LUC* expression without nitrate. CPK10(KM) lacking kinase activity and NLP7(S205A) lacking the CPK10, CPK30 and CPK32 phosphorylation site served as negative controls. NLP7 or CPK10ac protein expression was detected by immunoblot analyses before dividing protoplasts equally, and treated with 0.5 mM KCl or KNO_3 for 2 h. *UBQ10-GUS* is a transient expression control. Error bars, s.d., $n = 5$ biological replicates.

Extended Data Figure 8 | The CPK phosphorylation residue Ser205 is required for NLP7 nuclear retention triggered by nitrate at the plant root tip. a, CPK–GFPs are not processed in response to nitrate. Proteins from CPK–GFP-transfected protoplasts were analysed by immunoblots with an anti-GFP antibody. **b**, Confocal image of NLP7–GFP or NLP7(S205A)–GFP in transgenic *nlp7-1* complementation plants in response to nitrate. GFP images recorded at 0 or 8 min after 10 mM KNO_3 induction are shown. Scale bars, 100 μm. The experiments were repeated 3 times with 10 seedlings for each line with consistent results.
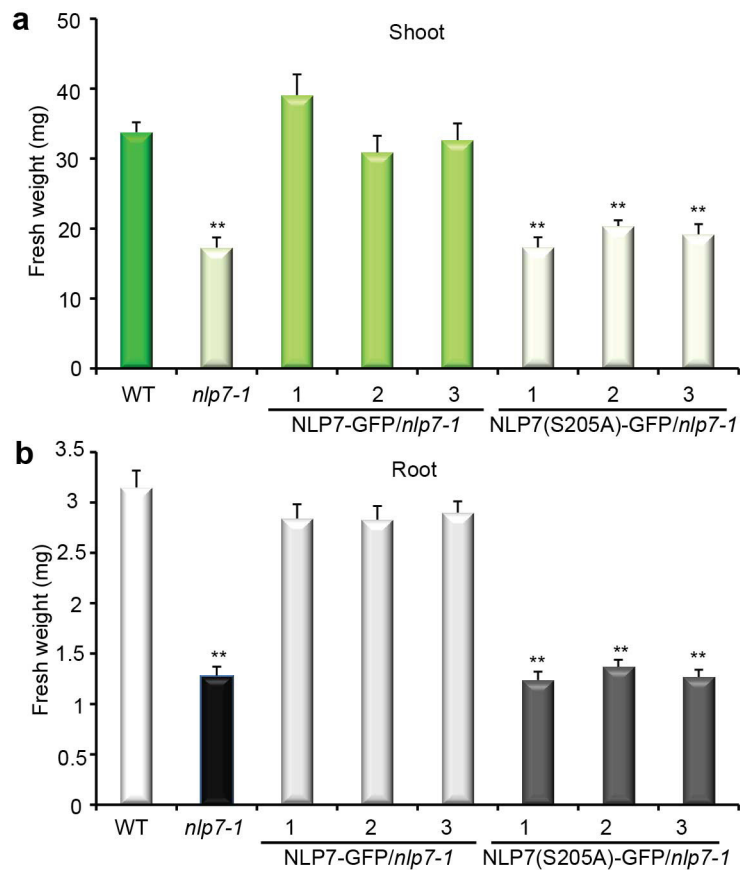
a

	NLP7	S205A	
HA			
			NIR
			NIA1
			LBD37
			LBD38
			FNR2
			NRT2.1
			MAPKKK13
			PGM
			ASR3
			TPPB

1 2 3
log₂ ratio

b

	NLP7	S205A	
			MCM2
			MCM3 — Cell cycle
			ETG1
			CDC20.2
			ORC2
			TAR2 — Auxin regulation
			PIN7
			TMK1
			TUB4 — Control
			H2A

1 2 3
log₂ ratio

c

AGI number	Ctl-1	Ctl-2	NLP7-1	NLP7-2	NLP7-S205A-1	NLP7-S205A-2	Signal Log₂ ratio NLP7/Ctl	Signal Log₂ ratio NLP7-S207A/Ctl	Gene name
AT2G15620	6730	6992	38151	40155	8889	9936	2.4	0	*NIR*
AT1G77760	5591	6720	16383	17800	6165	6083	1.4	0	*NIA1*
AT5G67420	451	433	1870	1775	434	420	1.9	0	*LBD37*
AT3G49940	154	159	826	714	131	182	2.0	0	*LBD38*
AT1G30510	118	141	951	951	188	210	2.6	0	*FNR2*
AT1G08090	1	2	556	655	7	2	5.0	0	*NRT2.1*
AT1G07150	112	167	856	823	222	150	2.2	0	*MAPKKK13*
AT1G78050	123	123	5807	5697	231	268	5.2	0	*PGM*
AT2G33550	105	130	1829	1837	129	171	3.6	0	*ASR3*
AT1G78090	1	3	41	23	5	3	1.0	0	*TPPB*
AT1G44900	24	31	499	518	29	21	3.4	0	*MCM2*
AT5G46280	18	18	364	419	17	14	3.4	0	*MCM3*
AT2G40550	9	28	279	219	26	26	2.4	0	*ETG1*
AT4G33260	5	3	77	68	9	10	1.7	0	*CDC20.2*
AT2G37560	4	1	80	47	11	11	1.6	0	*ORC2*
AT4G24670	9	18	384	403	16	14	3.5	0	*TAR2*
AT1G23080	7	4	295	236	11	5	3.4	0	*PIN7*
AT3G24660	0	2	128	137	2	1	2.8	0	*TMK1*
AT5G44340	3474	3765	3403	3891	3601	3470	0.0	0	*TUB4*
AT3G20670	392	393	335	333	410	338	0.0	0	*H2A*

Extended Data Figure 9 | Nitrate enhancement of proliferation in the lateral root primordia. a, b, Ser205 is crucial for NLP7-mediated transcriptional activation of target genes with diverse functions. Genome-wide transcriptional profiling by RNA-seq was performed with mesophyll protoplasts expressing NLP7–HA or NLP7(S205A)–HA or the control plasmid for 4.5 h. Red, NLP7 target genes identified by both ChIP–chip[13] and DNA affinity purification sequencing (DAP-seq)[67]; black, ChIP–chip only; grey, DAP-seq only. **c**, Normalized HTSeq read counts of NLP7-activated genes (listed in **a** and **b**) from RNA-seq experiments. Normalized read counts of NLP7-activated genes calculated as the original HTseq counts divided by the normalization factors were extracted after DESeq2 analysis.

Extended Data Figure 10 | Complementation analyses of *nlp7-1* with NLP7–GFP or NLP7(S205A)–GFP in transgenic *Arabidopsis* plants. **a**, The shoot fresh weight of wild-type, *nlp7-1*, NLP7-GFP/*nlp7-1* and NLP7(S205A)–GFP/*nlp7-1* shoots. Error bars, s.e.m., $n = 10$ seedlings. **$P \leq 0.0001$ versus wild-type control (one-way ANOVA with Tukey's multiple comparisons test). Plants were grown on 25 mM KNO$_3$ medium for 21 days. Data from three independent complement lines are presented. **b**, The root fresh weight of 11-day-old wild-type, *nlp7-1*, NLP7–GFP/*nlp7-1* and NLP7(S205A)–GFP/*nlp7-1*. Seedlings were germinated on the ammonium succinate medium for 3 days and then transferred to the plates supplemented with 5 mM KNO$_3$ for 8 days. Error bars, s.e.m., $n = 10$ seedlings. **$P \leq 0.0001$ versus wild-type control (one-way ANOVA with Tukey's multiple comparisons test).